HHS Public Access

Author manuscript

Cell Rep. Author manuscript; available in PMC 2021 June 29.

Published in final edited form as:

Cell Rep. 2021 January 12; 34(2): 108624. doi:10.1016/j.celrep.2020.108624.

Endogenous Fatty Acid Synthesis Drives Brown Adipose Tissue Involution

Christian Schlein[1,13], **Alexander W. Fischer**[1,13], **Frederike Sass**[1], **Anna Worthmann**[1], **Klaus Tödter**[1], **Michelle Y. Jaeckstein**[1], **Janina Behrens**[1], **Matthew D. Lynes**[2], **Michael A. Kiebish**[3], **Niven R. Narain**[3], **Val Bussberg**[3], **Abena Darkwah**[3], **Naja Zenius Jespersen**[4], **Søren Nielsen**[4], **Camilla Scheele**[4,5], **Michaela Schweizer**[6], **Ingke Braren**[7], **Alexander Bartelt**[8,9,10,11], **Yu-Hua Tseng**[2,12], **Joerg Heeren**[1], **Ludger Scheja**[1,14,*]

[1]Department of Biochemistry and Molecular Cell Biology, University Medical Center Hamburg-Eppendorf, Hamburg, Germany

[2]Section on Integrative Physiology and Metabolism, Joslin Diabetes Center, Harvard Medical School, Boston, MA, USA

[3]BERG, Framingham, MA, USA

[4]Centre for Physical Activity Research, Rigshospitalet, University of Copenhagen, Copenhagen, Denmark

[5]Novo Nordisk Foundation Center for Basic Metabolic Research, Faculty of Health and Medical Sciences, University of Copenhagen, 2200 Copenhagen, Denmark

[6]Core Facility of Electron Microscopy, Center for Molecular Neurobiology ZMNH, University Medical Center Hamburg-Eppendorf, Hamburg, Germany

[7]Vector Facility, University Medical Center Hamburg-Eppendorf, Hamburg, Germany

[8]Department of Molecular Metabolism & Sabri Ülker Center, Harvard T.H. Chan School of Public Health, Boston, MA, USA

[9]Institute for Cardiovascular Prevention (IPEK), Ludwig-Maximilians-University, 81377 Munich, Germany

[10]German Center for Cardiovascular Research (DZHK), Partner Site Munich Heart Alliance, Munich, Germany

[11]Institute for Diabetes and Cancer (IDC), Helmholtz Center Munich, Neuherberg, Germany

*Correspondence: l.scheja@uke.de.

AUTHOR CONTRIBUTIONS

C. Schlein, A.W.F., J.H., and L.S. designed the study, researched data, and wrote the manuscript. F.S., A.W., M.D.L., M.A.K., N.R.N., V.B., A.D., K.T., A.B., J.B., M.S., I.B., M.Y.J., N.Z.J., and S.N. researched data and contributed to discussion. Y.-H.T. and C. Scheele helped design experiments and contributed to data discussion and interpretation. All authors read, edited, and approved the manuscript.

DECLARATION OF INTERESTS

The authors declare no competing interests.

SUPPLEMENTAL INFORMATION

Supplemental Information can be found online at https://doi.org/10.1016/j.celrep.2020.108624.

[12]Harvard Stem Cell Institute, Harvard University, Cambridge, MA, USA

[13]These authors contributed equally

[14]Lead Contact

SUMMARY

Thermoneutral conditions typical for standard human living environments result in brown adipose tissue (BAT) involution, characterized by decreased mitochondrial mass and increased lipid deposition. Low BAT activity is associated with poor metabolic health, and BAT reactivation may confer therapeutic potential. However, the molecular drivers of this BAT adaptive process in response to thermoneutrality remain enigmatic. Using metabolic and lipidomic approaches, we show that endogenous fatty acid synthesis, regulated by carbohydrate-response element-binding protein (ChREBP), is the central regulator of BAT involution. By transcriptional control of lipogenesis-related enzymes, ChREBP determines the abundance and composition of both storage and membrane lipids known to regulate organelle turnover and function. Notably, ChREBP deficiency and pharmacological inhibition of lipogenesis during thermoneutral adaptation preserved mitochondrial mass and thermogenic capacity of BAT independently of mitochondrial biogenesis. In conclusion, we establish lipogenesis as a potential therapeutic target to prevent loss of BAT thermogenic capacity as seen in adult humans.

In Brief

Schlein et al. show that carbohydrate-response element-binding protein (ChREBP) controls *de novo* lipogenesis (DNL) in brown adipose tissue (BAT) and determines BAT whitening in response to thermoneutral housing. ChREBP deficiency prevents enrichment of DNL-derived lipids and mitophagy during BAT involution, which is associated with higher thermogenic capacity.

Graphical Abstract

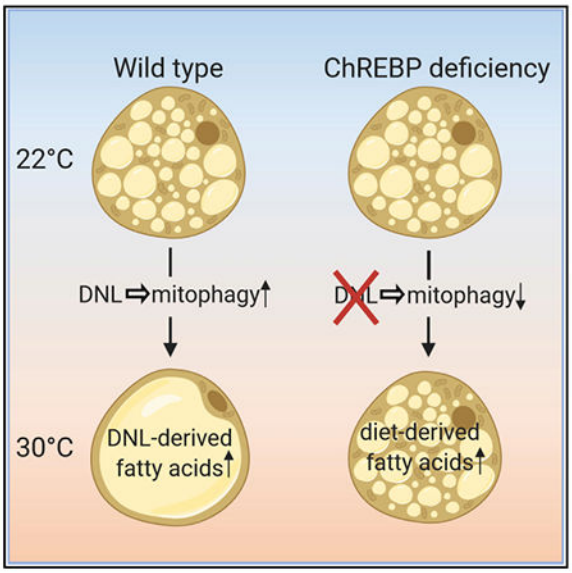

INTRODUCTION

The remarkable capacity for energy combustion of thermogenic brown adipocytes represents a valuable therapeutic target for treating obesity, dyslipidemia, and atherosclerosis (Bartelt and Heeren, 2012; Chen et al., 2020; Schlein and Heeren, 2016). Within BAT, in response to sympathetic stimulation, heat is produced via non-shivering thermogenesis through the inner mitochondrial membrane protein uncoupling protein 1 (UCP1), thereby significantly affecting whole-body metabolism (Cannon and Nedergaard, 2004). Numerous positron emission tomography/computer tomography (PET/CT) studies in healthy adult humans have demonstrated the presence of BAT, which can be activated and recruited by cold exposure or pharmacological intervention (Cypess et al., 2009,2015; Hany et al., 2002; Nedergaard et al., 2007; O'Mara et al., 2020; Saito et al., 2009; van der Lans et al., 2013; van Marken Lichtenbelt et al., 2009; Virtanen et al., 2009; Zingaretti et al., 2009). Importantly, lower or absent BAT PET/CT signals were detected in aged, obese, and/or insulin-resistant individuals (Cypess et al., 2009; Saito et al., 2009; van Marken Lichtenbelt et al., 2009), indicating that a decline in metabolic health correlates with reduced BAT activity. Importantly, although cold exposure can undoubtedly exert profound beneficial effects on human metabolism, most humans spend most of their lives under thermoneutral or near-thermoneutral conditions (Cannon et al., 2020; Fischer et al., 2018, 2019a).

Thermoneutrality is defined as the ambient temperature range where basal metabolism is sufficient to maintain body temperature, and thus no BAT recruitment or activity is needed. In mice, and presumably humans, prolonged living at thermoneutral temperatures results in BAT whitening, an involution process characterized by functional loss, lipid accumulation, and decreased mitochondrial mass in BAT (de Jong et al., 2019; Škop et al., 2020). One hallmark of BAT adaptation to thermoneutrality is the accumulation of triacylglycerols (TAGs) (de Jong et al., 2019) that can originate from several metabolic pathways. In BAT of cold-exposed mice, high amounts of lipids are taken up from circulating TAG-rich lipoproteins (TRLs) (Bartelt et al., 2011). Moreover, cold stimulates *de novo* lipogenesis (DNL), the synthesis of saturated and monounsaturated fatty acids from glucose-derived acetyl coenzyme A (CoA) (Mottillo et al., 2014). This synthetic pathway is regulated on the transcriptional level, especially by carbohydrate-response element-binding protein (ChREBP; encoded by *Mlxipl*) and sterol-regulatory element-binding protein 1 (encoded by *Srebf1*). In the liver, these transcription factors are equally important for the expression of DNL enzymes, such as ATP citrate lyase (encoded by *Acly*), acetyl CoA carboxylase α (encoded by *Acaca*), fatty acid synthase (encoded by *Fasn*), and elongases, such as elongation of very long-chain fatty acids protein 6 (encoded by *Elovl6*) and stearoyl-CoA desaturase 1 (encoded by *Scd1*) (Shimano and Sato, 2017; Wang et al., 2015). In adipose tissues, the contribution of each transcription factor to DNL gene expression is less well defined (Adlanmerini et al., 2019; Shimano and Sato, 2017; Vijayakumar et al., 2017). In the context of BAT whitening, it is important to note that at thermoneutrality, both TRL uptake and DNL are profoundly suppressed (Heine et al., 2018; Sanchez-Gurmaches et al., 2018), reflecting reduced energy demands of thermogenically inactive BAT. Therefore, the lipid source and the mechanisms underlying fat accumulation under this condition are unclear. Despite the clinical potential of BAT-related treatments for obesity-associated metabolic

diseases, the mechanisms underlying BAT whitening, and thus potential low therapy responsiveness, remain enigmatic.

Here, we report that BAT whitening is predominantly fueled by newly synthesized fatty acids accumulating within storage and membrane lipids and not by accretion of dietary fatty acids. This study introduces the concept of BAT involution as an active process driven by the lipogenic transcription factor ChREBP. ChREBP deficiency leads to a resistance to lipid accumulation and mitochondrial breakdown, and thus ChREBP-deficient mice are resistant to BAT involution, which can also be recapitulated by pharmacological inhibition of lipogenesis. In summary, we describe a pathway in BAT that allows to regulate and prevent BAT whitening.

RESULTS

Fatty Acid Synthesis Is Essential for BAT Whitening

Adaptation of mice to thermoneutrality (30°C) leads to increased lipid accumulation and decreased UCP1 density in BAT (Figure 1A). Residual UCP1 staining was observed in thermoneutral BAT, indicating that the cellular identity of brown adipocytes is preserved under this condition. To elucidate the source of the accumulating lipids, we performed fatty acid profiling using gas chromatography and calculated the ratio of palmitoleic acid (16:1) to linoleic acid (18:2), a marker of the amount of endogenously synthesized versus dietary fatty acids. This lipogenic index was increased in thermoneutral BAT in both TAGs (Figure 1B) and phospholipids (Figure 1C) after housing at thermoneutrality for 1 or 4 weeks, demonstrating higher use of endogenous fatty acids for synthesis of complex lipids. Of note, the higher relative contribution of DNL versus exogenous fatty acids to cellular fatty acid pools occurred despite decreased expression of *Chrebp-beta,* a main regulator of lipogenesis in human and mouse adipose tissues (Eissing et al., 2013; Herman et al., 2012; Vijayakumar et al., 2017), its lipogenic target genes encoded by *Acly, Acaca, Fasn, Scd1,* and *Elovl6,* as well as to a smaller extent the lipogenic transcription factors of the SREBP family in thermoneutral BAT (Figure S1A). As expected, expression of markers of thermogenesis and mitochondrial biogenesis markers was decreased at thermoneutrality in an acclimation time-dependent manner (Figure S1A). The absolute expression levels of *Chrebp-alpha* were 2-fold higher compared with the *Chrebp-beta* isoform (Figure S1B). To investigate whether increased endogenously produced fatty acids have an impact on the BAT involution process, we acclimated ChREBP-deficient (ChREBP-knockout [KO]) mice and their wild-type littermates to 30°C. The total ChREBP-KO mice lack exons 12–14 and, therefore, have no DNA-binding activity (Iizuka et al., 2004). The expression data indicate that the truncated version of *Chrebp-alpha* mRNA is still expressed in ChREBP KO to a similar level as the wild-type version (Figure 1D). *Chrebp-alpha* mRNA can be detected in the KO mice because the qPCR was designed to detect the exon 1a/exon 2 boundary, which is not deleted in the KO mice. Importantly, the expression of lipogenesis genes in BAT of ChREBP-KO mice housed at thermoneutrality and room temperature was markedly reduced compared with wild-type controls (Figure 1D). The expression levels of *Srebf1, Srebf2,* and *Srebp1c* were not significantly affected. Because expression of DNL genes such as *Acly, Acaca,* and *Fasn* is markedly reduced in BAT of ChREBP-KO mice, these data indicate that the SREBP

family members at least under this condition are not able to compensate for the loss of ChREBP in regulating DNL genes in BAT. Glucose influx increases ChREBP activity (Wang et al., 2015); thus, we also compared the expression of these genes under fasting and refeeding conditions in BAT of wild-type and ChREBP-KO mice. Refeeding resulted in higher *Chrebp-beta, Fasn,* and *Acaca* gene expression in wild-type mice, whereas ChREBP-KO mice exhibited a loss of response to refeeding in lipogenesis-associated gene expression (Figure S1C). The levels of *Chrebp-alpha* and *Srebf2* were unaffected by fasting-refeeding or ChREBP deletion, whereas the expression of *Srebf1* and especially *Srebp1c* was increased upon refeeding, an effect that was attenuated in ChREBP-KO mice (Figure S1C). Thermogenic gene expression was unaltered or reduced upon refeeding (Figure S1C). SREBP1c activity and expression are regulated by insulin in the liver, whereas ChREBP is activated by glucose influx that subsequently triggers generation of ChREBP-activating glucose-derived metabolites (Abdul-Wahed et al., 2017; Jeon and Osborne, 2012). To assess how insulin signaling would affect lipogenesis in BAT, we utilized inducible BAT-specific insulin receptor KO mice and measured lipogenic gene expression (Figure S1D). We observed reduced levels of DNL genes in the KO mice, whereas thermogenic marker expression was largely unaltered (Figure S1D). Interestingly, among the transcription factors, only *Chrebp-beta* was affected and showed a trend for lower expression in the absence of the insulin receptor (Figure S1D), consistent with insulin-dependent glucose transport controlling ChREBP activity (Herman et al., 2012). Taken together, these data indicate that ChREBP is the predominant lipogenic transcription factor in BAT, especially in the postprandial situation. Supporting this notion, ChREBP-KO mice also displayed a strongly reduced lipogenesis index in both TAGs (Figure 1E) and phospholipids (Figure 1F). Importantly, the mice had been acclimated to thermoneutrality for 12 weeks, a longer period of lipid remodeling compared with those shown in Figures 1B and 1C, which leads to further increases of the lipogenic index.

To elucidate whether ChREBP is also linked to lipogenic gene expression in human BAT, we examined gene expression relationships in an already established RNA sequencing (RNA-seq) dataset (Jespersen et al., 2020). This dataset was composed of BAT isolated from a cohort of normal weight, overweight, and obese human subjects, where overweight and obesity were reported to associate with a decline in mitochondrial and thermogenic gene expression (Jespersen et al., 2020). Cohorts of lean and obese subjects are known to show a great variety in ChREBP-beta expression and lipogenesis (Eissing et al., 2013), which allows to correlate its expression to its putative targets. Therefore, these data were deemed suitable to determine the importance for ChREBP (encoded by the human gene *MLXIPL*) for BAT lipogenesis. The data do not allow to discriminate between ChREBP isoforms, which would be necessary to more precisely estimate ChREBP transcriptional activity. Nevertheless, *MLXIPL* gene expression correlated with the expression of the lipogenic genes *ACLY* (Figure 1G), *ACACA* (Figure 1H), *FASN* (Figure 1I), and *SCD* (Figure 1J), consistent with a role of ChREBP in lipogenic gene expression also in human BAT.

Next, we investigated whether the loss of fatty acid synthesis in ChREBP-KO mice affects the course of BAT whitening. Histological analysis revealed markedly decreased lipid deposition and also pronounced UCP1 immunostaining in BAT of thermoneutral ChREBP-KO mice (Figure 1K), arguing for a preservation of thermogenic potential. Supporting this

notion, protein levels of UCP1 and mitochondrial oxidative phosphorylation complexes (OXPHOS) were strongly decreased in whitened BAT of wild-type mice. Of note, we detected higher levels of these proteins in BAT of thermoneutral ChREBP-KO mice (Figures 1L and S1E). In line, electron microscopy analysis showed higher mitochondrial numbers in ChREBP-KO mice even after prolonged acclimation to thermoneutrality, which was also reflected by a more brownish macroscopic appearance of the tissue (Figures 1M and S1F). Of note, the levels of mitochondria were still relatively high in BAT of the wild-type controls after the 12-week thermoneutral adaptation, indicating preserved cellular identity of the brown adipocytes. Consistent with the higher respiratory chain complex and UCP1 content, mitochondria isolated from BAT of ChREBP-KO mice displayed higher maximal (CCCP-induced) and UCP1-dependent (GDP-sensitive) respiration compared with mitochondria from BAT of wild-type controls (Figures 1N and S1G). Moreover, BAT activation by refeeding, an intervention known to provoke diet-induced thermogenesis (Li et al., 2018; von Essen et al., 2017), and subsequent beta3-adrenergic stimulation using the selective agonist CL316,243 revealed higher oxygen consumption in ChREBP-KO than in wild-type mice (Figures S1H and S1I). The reduction in oxygen consumption following the initial refeeding bout most likely reflects cessation of food intake after the initial excitement period (von Essen et al., 2017). Altogether, ChREBP deficiency reduces thermoneutrality-induced BAT whitening, which is associated with preserved mitochondrial mass and function.

Similar to the effects of ChREBP deficiency, administration of the allosteric acetyl-CoA carboxylase (ACC) inhibitor (ACCi) CP-640186 (Harwood et al., 2003) during adaption to thermoneutrality resulted in markedly reduced lipid accumulation in BAT (Figure 1O). As observed in ChREBP-deficient mice, BAT UCP1 protein levels were partially preserved in ACCi-treated mice acclimated to thermoneutrality (Figures 1P and S1J). In line with these findings, inhibition of ACC resulted in higher BAT thermogenic capacity, measured as oxygen consumption in response to beta3-adrenergic stimulation in mice adapted to 30°C (Figures S1K and S1L).

In conclusion, endogenous synthesis of fatty acids is essential for BAT whitening, and targeting this pathway by genetic or pharmacological approaches prevents the decline in thermogenic capacity at thermoneutrality, which prepares the tissue for activation by diet or adrenergic stimulation.

Reduced Endogenous Fatty Acid Species in ChREBP-KO Mice Despite Higher Uptake of Dietary Lipids

Activated brown adipocytes internalize high amounts of glucose and TAGs to meet their energetic demands (Bartelt et al., 2011; Heine et al., 2018). To investigate whether the reduced lipid accumulation observed in BAT of thermoneutral ChREBP-KO mice was secondary to reduced dietary uptake, we performed a combined oral glucose and fat tolerance test with radioactively labeled ^{3}H-deoxyglucose and ^{14}C-triolein. At housing temperatures of both 22°C and 30°C, BAT of ChREBP-KO mice exhibited a 2-fold higher uptake of ^{14}C-triolein uptake compared with wild-type littermates, whereas uptake into white fat and other lipoprotein-processing organs was largely unaffected (Figure 2A). In contrast, ^{3}H-deoxyglucose uptake was diminished in both white and brown fat of ChREBP-

KO mice compared with wild-type controls housed at 22°C, but not 30°C, whereas uptake into the liver and the heart was increased (Figure 2B). Notably, glucose and lipid uptake in BAT correlated with one another in wild-type, but not ChREBP-KO, mice (Figure 2C), implicating an important role of ChREBP in balancing energy substrate utilization in brown adipocytes. In line with increased lipid uptake, the abundance of mainly diet-derived polyunsaturated fatty acids was higher in both phospholipids and TAGs, as well as in mitochondrial lipid extracts from BAT of ChREBP-KO mice (Figure 2D). In accordance with the reduced lipogenesis index in ChREBP-KO mice (Figures 1E and 1F), the levels of mainly endogenously produced monounsaturated fatty acids were decreased in TAGs, phospholipids, and mitochondrial lipid extracts (Figure 2D), emphasizing a strong effect on both storage and membrane lipids. Thus, the reduced lipid deposition in BAT of thermoneutral ChREBP-KO mice cannot be explained by reduced lipid uptake. Lipid uptake is rather increased in these mice, leading to a proportionally higher incorporation of dietary polyunsaturated fatty acids.

Loss of Endogenous Lipid Production Leads to Diminished Organelle Degradation

The higher mitochondrial abundance upon loss of lipogenesis in thermoneutral BAT could be caused by elevated sympathetic tone. Arguing against this, expression of cAMP-dependent genes, such as *Ucp1* and *Dio2* (Figure 3A), as well as protein kinase A substrate phosphorylation determined by western blot analysis (Figure S2A), was similar between the genotypes. Likewise, expression of mitochondrial biogenesis and oxidative phosphorylation genes, such as *Ppargc1a, Tfam,* and *Cox4i1,* in BAT was unaffected by ChREBP deficiency (Figure 3A).

To rule out any potential confounding effects of sympathetic nerve activity, we denervated BAT to induce whitening of the tissue (Fischer et al., 2019b). In the sham-operated mice, basal UCP1 levels were higher in ChREBP-deficient mice compared with wild-type controls (Figures 3B and 3C). Denervation reduced UCP1 levels in both genotypes, but it is of note that UCP1 protein levels were still higher in ChREBP-KO mice than in wild-type controls (Figures 3B and 3C). These data indicate that the prevention of BAT involution observed in ChREBP deficiency is retained after cessation of adrenergic signaling. Taken together, these findings demonstrated that the increased mitochondrial levels in BAT of thermoneutral ChREBP-KO mice were not due to elevated mitochondrial biogenesis. Because the whitening of BAT is associated with profound loss of mitochondria (see control mice in Figures 1L and 1M), we hypothesized that ChREBP-mediated lipogenesis might be important for the regulation of the breakdown of mitochondria and mitochondrial proteins. The proteasome is one of the major mediators of protein degradation, and its activity has been previously shown to be reduced under thermoneutral conditions (Bartelt et al., 2018). This was, however, not affected by ChREBP deficiency (Figure S2B). We therefore tested the hypothesis that autophagy might be important for mitochondrial degradation in BAT at thermoneutrality. Indeed, treatment of wild-type mice with wortmannin, which blocks autophagy through phosphatidy-linositol-3-kinase inhibition (Blommaart et al., 1997; Yang et al., 2013), resulted in a strong increase in UCP1 protein (Figure S2C) and prevented BAT whitening during adaptation to 30°C (Figure S2D). Evidence for alterations in the autophagic pathway in ChREBP-KO mice was provided by histological analysis

demonstrating significantly more LC3 punctae in BAT of wild-type versus ChREBP-KO mice housed at thermoneutrality (Figures 3D–3G), indicating a higher number of mature autophagosomes in wild-type than in ChREBP-KO, BAT. This was demonstrated by anti-LC3 immunostaining (Figures 3D and 3E) and by an alternative approach using an adeno-associated virus vector encoding a fluorescent chimera of LC3 (Klionsky, 2011) Figures 3F and 3G). In sum, we provide evidence that mitochondrial breakdown via autophagy determines BAT whitening in a ChREBP-dependent manner.

Lipogenesis Is Required for Remodeling of Membrane and Storage Lipids at Thermoneutrality

To determine compositional changes in cellular lipids and thus identify lipid species that may potentially act as mediators of BAT whitening, we performed a broad lipidomic analysis in BAT of wild-type and ChREBP-KO mice at 22°C and 30°C (Figure 4A). In line with differences in BAT whitening between genotypes (Figure 1), the total concentrations of TAGs, diacylglycerols (DAGs), and cholesterol esters (CEs) were increased in BAT of thermoneutral wild-type, but not ChREBP-KO, mice (Figure 4A, left panel). In contrast, the levels of phospholipids were decreased in thermoneutral BAT of wild-type mice, consistent with reduced levels of mitochondria and other organelles in inactive BAT. ChREBP-KO mice also displayed such decrease, yet in certain lipid classes such as mitochondrial cardiolipins (CLs) to a lower extent. To elucidate the incorporation of endogenously produced versus dietary lipids in more detail, we calculated the levels of lipids enriched in mainly endogenously produced C_{14}-C_{16} fatty acids and such enriched in dietary 18:2 (Figure 4A, middle and right panels). The abundance of DAG and TAG, as well as major phospholipid classes such as phosphatidylcholine (PC) and CLs, enriched in C_{14}-C_{16} fatty acids was strongly increased in thermoneutral BAT of wild-type, but not in ChREBP-KO, mice. In contrast, dietary linoleic acid was enriched in CLs and several membrane lipid classes in BAT of ChREBP-KO mice as compared with wild-type controls (Figure 4A, right panel). These findings show a strong remodeling in fatty acid composition of not only storage but also important membrane lipid classes, including CLs in wild-type, but not ChREBP-KO, mice upon thermoneutral adaptation. The total amount of TAGs correlated negatively with CL content, reflecting increased lipid accumulation in BAT with low mitochondrial content, and vice versa (Figure 4B). In contrast, the levels of CLs and TAGs enriched in mainly endogenously produced C_{14}-C_{16} fatty acids correlated positively (Figure 4C) and were both higher in wild-type (black dots) than in ChREBP-KO mice (white dots). This indicates that the remodeling of both lipid classes upon whitening is dependent on lipogenesis, because it happened only in wild-type mice and suggests a specific function of C_{14}-C_{16} fatty acid residues in membrane and storage lipids.

Excess Dietary Lipids Disconnect Lipid Storage from Mitochondrial Breakdown

We challenged both wild-type and ChREBP-KO mice with exogenous lipids by high-fat diet (HFD) feeding at 30°C, aiming to provide an excess amount of (especially saturated and mono-unsaturated; Figure S3A) fatty acids to override the BAT phenotype of ChREBP-deficient mice observed at thermoneutrality. While wild-type mice housed at thermoneutrality fed a chow diet displayed an increase in TAG species containing fatty acids with either 0, 1–5, or ≥6 double bonds (Figure 5A), ChREBP-KO mice showed a blunted

response specifically in TAG species containing, predominantly endogenously produced saturated (0) or low-desaturated fatty acids (1–5), whereas species with highly unsaturated fatty acids (≥6) were increased (Figure 5A). Upon HFD challenge, the levels in unsaturated and low desaturated fatty acid residues were increased in ChREBP-KO mice, rendering them more similar to wild-type mice and proving that a rescue of the reduced levels in endogenously produced fatty acids in thermoneutral BAT of ChREBP-KO mice by dietary supplementation was possible (see also Figure S3B). An excess of exogenous fatty acids rescued the lipid phenotype of ChREBP-deficient BAT (Figure 5B). BAT protein levels of UCP1 and OXPHOS proteins were comparable between genotypes after the HFD challenge in ChREBP-KO and wild-type mice (Figures S3D and S3E). In line with previous findings (Feldmann et al., 2009; Fischer et al., 2019b), HFD feeding led to a strong increase in UCP1 and OXPHOS levels in wild-type mice to an equally high level of UCP1 as seen in ChREBP-KO BAT (Figures S3D and S3E), whereas gene expression of *Ucp1* was increased equally in both wild-type and ChREBP-deficient mice (Figure S3F). This indicates that HFD feeding blocks DNL, leveling the turnover rate of mitochondria of wild-type and ChREBP-KO mice, which is supported by the normalized lipogenesis-derived CL residues, as well as the CL lipidome (Figures 5C and S3C).

To study this process in a cell-type-specific manner and to rule out potential effects caused by ChREBP loss in non-adipocytes, we crossed mice expressing Cre recombinase under the control of the *Ucp1* promoter (*Ucp1-Cre*) with *Mlxipl*$^{flox/flox}$ mice (Jois et al., 2017). The gene expression of *Chrebp-beta* and lipogenesis enzymes was markedly lower in *Ucp1-Cre*$^{+}$ *Mlxipl*$^{flox/flox}$ (Cre^{+}) compared with *Ucp1-Cre*- *Mlxipl*$^{flox/flox}$ (Cre^{-}) mice kept at 22°C or 30°C (Figure S4A), whereas thermogenic and mitochondrial gene expression was largely unaffected at thermoneutrality (Figure S4B). In line with results obtained using the whole-body ChREBP-KO mice, Cre^{+} mice showed reduced lipid deposition within BAT upon thermoneutral housing (Figure 5D), which was accompanied by higher UCP1 and OXPHOS protein levels (Figures 5E and S4C). To verify the loss of ChREBP protein in both KO models, we analyzed protein expression in BAT of mice acclimated to thermoneutrality (Figure S4D). Both models, global and BAT-specific KOs, displayed a marked decrease in ChREBP protein levels. Residual ChREBP protein in *Ucp1-Cre*$^{+}$ *Mlxipl*$^{flox/flox}$ (Cre^{+}) mice most likely reflects expression in non-adipocytes. These data confirm that the seemingly unchanged expression of *Chrebp-alpha* in global KO mice (Figures 1D and S1C) represents a truncated mRNA(due to loss of exons 12–14) (Iizuka et al., 2004), not giving rise to functional ChREBP protein. We observed an enrichment of endogenously produced C_{16}-fatty acid-containing lipid species observed in thermoneutral BAT of Cre^{-} mice, but not in Cre^{+} mice (Figure S4E). In line with the findings obtained in global ChREBP-KO mice, lipid uptake into BAT of *Ucp1-Cre*$^{+}$ *Mlxipl*$^{flox/flox}$ (Cre^{+}) mice was increased (Figure S4F), whereas glucose uptake was decreased (Figure S4G). Importantly, these results also show that this phenotype observed in global ChREBP-KO mice is not the result of altered intestinal absorption of dietary glucose and lipids or other systemic alterations but rather an intrinsic characteristic of ChREBP-deficient BAT. In line with these findings, Cre^{+} mice displayed an enrichment of dietary 18:2-enriched lipid species (Figure S4E). These effects were not restricted to TAGs (Figure S4J) but were also observed in phospholipids, such as PCs (Figure S4H), phosphatidylethanolamines (Figure S4I), and CLs (Figure S4K). Overall,

these data recapitulate the results obtained in global ChREBP deficiency, providing evidence for a cell-autonomous effect of ChREBP deficiency in resistance to BAT whitening. Altogether, these data show a massive remodeling of structural and storage lipids upon thermoneutral adaptation. Incorporation of diet-derived fatty acids is decreased in favor of endogenously produced fatty acids. This process does not take place in ChREBP-deficient mice and is regulated in a tissue-autonomous level because it was observed in both global and BAT-specific ChREBP-deficient mice and thus cannot be compensated by lipogenesis of other organs, such as the liver. HFD feeding also rescued the lipid accumulation (Figure 5F) and the UCP1 and OXPHOS protein levels (Figures 5G and S4L) in BAT of thermoneutral-housed Cre^+ mice.

Thus, the protective effect of brown adipocyte ChREBP deficiency on BAT lipid accumulation can be outweighed by excessive dietary lipids, which prevents the distinct changes taking place on chow diet that are associated with higher mitochondrial turnover (see model in Figure 5H).

DISCUSSION

It is well established that housing temperatures determine the expression of lipogenic enzymes and thus fatty acid synthesis in thermogenic adipocytes. Cold exposure markedly increases lipogenesis (Trayhurn, 1981), and it has been proposed that this process is important for heat production through futile cycling of fatty acid synthesis and oxidation (Mottillo et al., 2014). Therefore, models of altered BAT lipogenesis have mainly been studied in the context of their response to cold (Adlanmerini et al., 2019; Sanchez-Gurmaches et al., 2018; Wei et al., 2020). A main research question highly relevant for human BAT pathophysiology (Cannon et al., 2020; de Jong et al., 2019; Ganeshan and Chawla, 2017; Scheele and Wolfrum, 2020), namely, the role of lipogenesis for BAT whitening during adaptation to thermoneutrality, has not been addressed so far. A key observation of our study is that at thermoneutrality, endogenously produced fatty acids have an increased contribution to the BAT lipid pool and play distinct roles in the remodeling of the tissue. So far, the role of fatty acids in the regulation of mitochondrial breakdown has been addressed in only a few studies. It was demonstrated that exogenous palmitate is a strong inducer of autophagy in various cell types (Komiya et al., 2010). Furthermore, SCD1-dependent conversion of palmitate to palmitoleate was necessary for palmitate-induced autophagy in a pancreatic beta cell line (Janikiewicz et al., 2015). In addition, loss of ACC has been shown to impair autophagy in yeast, an effect that could be rescued by supplying exogenous monounsaturated fatty acids (Gross et al., 2019). Those results are in line with our observations showing that thermoneutral housing ChREBP dependently raises monounsaturated fatty acid levels in various lipid classes of BAT. It has to be noted that in this study, we do not directly assess the relative contribution of the alpha and beta isoform of ChREBP independently. While our global mouse model lacks exons shared between both isoforms, the tissue-specific model lacks the alpha-specific exon. Our data indicate that loss of functional ChREBP-alpha is sufficient to blunt lipogenic gene expression in BAT, and we found that ChREBP-alpha is essential for the expression of ChREBP-beta in BAT. Thus, future studies are warranted to determine the specific contribution of ChREBP-beta to lipogenic gene expression and BAT whitening.

Notably, next to TAGs, most profound changes were detected in the composition of CLs. These lipids have been shown to influence mitophagy, because their translocation to the outer mitochondrial membrane can trigger mitochondrial turnover in cultured cells (Chu et al., 2013; Hsu et al., 2015). We observed a reduction in CLs containing dietary polyunsaturated fatty acids in thermoneutral BAT of wild-type, but not ChREBP-deficient, mice. Notably, CLs containing the dietary fatty acid linoleate have been shown previously to also be reduced in aged rat heart, while CLs containing endogenously produced fatty acids such as palmitic acid (16:0) were increased (Lee et al., 2006). Similarly, a reduction in CLs containing linoleate has been observed in a plethora of physiological and pathogenic conditions, including muscle inactivity (Fajardo et al., 2017), pulmonary hypertension (Saini-Chohan et al., 2011), heart failure (Saini-Chohan et al., 2009; Sparagna et al., 2007), and type 1 diabetic myocardium (Han et al., 2007). This is in line with our data showing a decline of CLs containing linoleate in thermogenically inactive mitochondria of thermoneutral BAT. In addition, due to the different fluidity and physicochemical properties of their acyl chain, polyunsaturated fatty acids have been shown to have profound effects on membrane curvature (Epand, 1998; Koenig et al., 1997; Smaby et al., 1997), thereby affecting mitochondrial function (Schenkel and Bakovic, 2014; Stanley et al., 2012; Sullivan et al., 2018). Our data suggest that enrichment of ChREBP-dependent, lipogenesis-derived fatty acids in CL species at the expense of dietary fatty acids could affect mitochondrial degradation in brown adipocytes of wild-type mice adapted to thermoneutrality. However, it is also conceivable that autophagic membranes, which are formed during the process of engulfment of the target organelle, may be formed out of DNL-derived lipids. Evidence for such a process has been recently described in yeast. In this study, it was demonstrated that autophagic membrane formation is dependent on acyl-CoA provided by fatty acid synthase (Schütter et al., 2020). In line, we observed lower amounts of autophagosomes detected as LC3-positive punctae in ChREBP-deficient BAT, which supports the general concept that autophagosome biogenesis and thus mitophagy depend on DNL.

The overall importance of mitophagy for mitochondrial clearance has so far mainly been shown in white adipose tissue, where the transition from a beige to a white adipocyte phenotype has been analyzed in detail by elegant *in vivo* lineage tracing experiments (Rosenwald et al., 2013) and studies assessing autophagic fluxes *in vivo* (Altshuler-Keylin et al., 2016; Lu et al., 2018). In these studies, the relevance of mitophagy for beige-to-white adipocyte transition was demonstrated by cell-type-specific deletion of the autophagy-related proteins ATG5 or ATG12.

In conclusion, we show that ChREBP-dependent expression of lipogenic enzymes is essential for BAT whitening. We provide direct evidence from pharmacological and genetic intervention studies that endogenous fatty acid synthesis promotes complex lipid remodeling, ultimately affecting mitochondrial breakdown. Loss of lipogenesis during thermoneutral adaptation preserves mitochondrial levels and impairs lipid accumulation. Importantly, the retained mitochondria appear healthy and functional as they can be activated *in vivo* and *ex vivo.* At least in mice the whitening process can be inhibited pharmacologically, establishing BAT whitening as a potential therapeutic target.

STAR★METHODS

RESOURCE AVAILABILITY

Lead Contact—Further information and requests for reagents may be directed to and will be fulfilled by the Lead Contact, Ludger Scheja (l.scheja@uke.de).

Materials Availability—This study did not generate new unique reagents.

Data and Code Availability—The published article includes all datasets generated or analyzed during this study.

EXPERIMENTAL MODEL AND SUBJECT DETAILS

Mice—All animal studies were performed with permission of the Animal Welfare Officers at University Medical Center Hamburg-Eppendorf or in accordance with approved institutional protocols of the Harvard T.H. Chan School of Public Health (HSPH) Institutional Animal Care and Use Committee. *Mlxipl*$^{flox/flox}$ mice were a kind gift of M.W. Sleeman (Monash University, Victoria, Australia) and Lawrence C. B. Chan (Baylor College of Medicine, Houston, Texas). All other mouse lines were purchased from Jackson Laboratories. DIO mice were kept on a high fat diet (Bio-Serv3282). Unless indicated otherwise, age and weight-matched male mice (8-20 weeks) were used. Routinely, mice were kept in single cages during adaptation to 22°C or 30°C in Memmert climate chambers with *ad libitum* access to food and water. Blood for EDTA plasma measurements was collected by tail vein blood withdrawal or cardiac puncture of anaesthetized mice.

Human subjects—BAT was isolated from a cohort of normal weight, overweight and obese human subjects as published (Jespersen et al., 2020). The 31 subjects included in this study were 23 women and 8 men, median age 55 (range: 23 - 74) years. The study was approved by the Scientific-Ethics-Committee of the Capital Region of Denmark, journal number: H-1-2014-015 and was conducted in accordance with the Helsinki declaration. All participants provided informed consent prior to participation in the study.

METHOD DETAILS

Pharmacological treatments—For pharmacological intervention studies, mice received daily intraperitoneal injections of 1 mg/kg wortmannin (Calbiochem) or 5 mg/kg CP-640186 (Sigma) in 10% DMSO, 90% saline for 7 days. Mock controls received vehicle only.

Metabolic tracer studies—For oral glucose and fat tolerance tests (OGFT), mice were fasted for 4 hours before receiving an oral gavage of 200 μL of a solution containing glucose (2 g/kg body weight) and triacylglycerol-rich lipoproteins (80 mg triacylglycerol/kg body weight), traced with ^{3}H-deoxy-glucose (0.72 MBq/kg body weight) and ^{14}C-triolein (0.15 MBq/kg body weight) . Two hours after gavage, organs were harvested after systemic perfusion with PBS-heparin (10U/ml) via the left heart ventricle. Tissues were solubilized for counting using Solvable and counted in a TriCarb scintillation counter (Perkin Elmer).

Denervation of brown adipose tissue—Denervation of brown adipose tissue (BAT) was performed as previously described (Fischer et al., 2019b). Briefly, mice were injected with 5 mg/kg carprofen and anaesthetized with 4% isoflurane inhalation in O_2. The interscapular region was shaved, sterilized with 80% ethanol and the skin was opened in a 1 cm incision. The BAT was carefully lifted up without puncturing the Sulzer's vein and the nerves were prepared. In one lobe, 5 nerves were cut, while in the contralateral lobe, the nerves were only touched and handled without cutting them. The skin incision was closed, and the animals were allowed to recover for 1 week at room temperature.

Histochemistry—Hematoxilin-Eosin staining was performed on paraffin embedded tissues. Briefly, sections (5 μm) were cut on a Leica Microtome and mounted on Histobond slides (Marienfeld-Superior). After de-paraffinization and rehydration, slides were incubated for 2 min in Hematoxilin, then blued under running tap water for 10 min, and counterstained with 0.5% Eosinfor 15 s. Afterward, the slides were dehydrated and mounting was performed using Eukitt. Microscopy was performed on a Nikon A1 Microscope equipped with a DS-U3 camera (Nikon).

Gene expression analysis—RNA was isolated from tissues using peqGOLD TriFast, by homogenizing tissues with a TissueLyser (QIAGEN) and purifying RNA by NucleoSpin RNAII Kit. Afterward, cDNA was prepared with High-Capacity cDNA Archive Kit. Gene expression was assessed using Taqman assays supplied as assays-on-demands, and data were normalized to the gene expression levels of the housekeeper *Tbp.*

Electron microscopy—Mice were transcardially perfused with a mixture of 4% paraformaldehyde and 1% glutaraldehyde in 0.1 M PB buffer at pH 7.4. Interscapular BAT was removed, and small pieces were prepared with a razor blade. The samples were rinsed three times in 0.1 M sodium cacodylate buffer (pH 7.2–7.4) and osmicated using 1% osmium tetroxide in cacodylate buffer. Following osmication, the samples were dehydrated using ascending ethyl alcohol concentration steps, followed by two rinses in propylene oxide. Infiltration of the embedding medium was performed by immersing the pieces in a 1:1 mixture of propylene oxide and Epon and Anally in neat Epon and hardened at 60°C. Semithin sections (0.5 μm) were prepared for light microscopy mounted on glass slides and stained for 1 minute with 1% Toluidine blue. Ultrathin sections (60 nm) were cut and mounted on copper grids. Sections were stained using uranyl acetate and lead citrate. Thin sections were examined and photographed using an EM902 (Zeiss) electron microscope. Quantification of mitochondrial content was performed using ImageJ.

Tissue lysates & western blotting—For western blotting, organs were dissected and snap-frozen immediately. Tissues were homogenized in 10x (v/w) RIPA buffer (50 mM Tris-HCI pH7.4; 5 mM EDTA; 150 mM NaCl; 1 mM Na-Pyrophosphate; 1 mM NaF; 1 mM Na-Vanadate; 1% NP-40) supplemented with cOmplete Mini Protease Inhibitor Cocktail Tablets (Roche) in a TissueLyser (QIAGEN) at 20 Hz for 2x3 min. The homogenate was centrifuged at 13,000 rpm for 10 min at 4°C and the supernatant was taken using a syringe and a 27G needle to avoid contamination from the upper fat layer. Protein concentration was determined using the BCA method. Protein lysates were diluted in NuPAGE® LDS Sample

buffer + Sample Reducing Agent; Invitrogen and 20 μg of total protein were separated in 10% or 12.5% Tris-Glycine SDS-PAGE. Transfer to nitrocellulose membranes (GE) was performed in a wet blotting system in blotting buffer (20 mM Tris, 150 mM Glycine, 20% (v/v) Methanol) for 2 h at 400 mA or overnight at 200 mA. Membranes were stained with Ponceau Red (Sigma), cut and blocked for 1 h in 5% milk in TBS-T (20 mM Tris, 150 mM NaCl, 0.1% (v/v) Tween 20). Membranes were incubated overnight at 4°C in the corresponding primary antibodies in 5% BSA (Sigma) in TBS-T. After washing 3 × 10 min in TBS-T, membranes were incubated for 1 h at RT in the corresponding HRP-conjugated secondary antibodies in 5% milk in TBS-T. After additional 3 × 10 min washing in TBS-T, detection was performed using SuperSignal West Femto ECL. For detection, either Amersham Hyperfilm system (GE) or Amersham Imager 600 (GE) were used. Quantification was performed using Li-Cor Image Studio Lite.

Indirect calorimetry—Indirect calorimetry was performed in a PhenoMaster System (TSE Systems) in a temperature- and humidity-controlled chamber as described before (Fischer et al., 2019b). After calibration of the oxygen and carbon dioxide sensors, oxygen consumption and carbon dioxide production were measured every 21 min. During the experiments, the mice were housed in their home cages at a 12 h/12 h light-dark cycle with free access to food and water. Before start of the respective experiment, the mice were allowed to acclimate to the system for at least 24 h. To analyze the effects of feeding as well as the response to the β3-adrenergic agonist CL316,243 on oxygen consumption, the mice (after acclimation to the chambers at 30°C) were fasted for 16 h overnight and then re-fed for 3 h before they were injected subcutaneously with 1 mg/kg CL316,243 in saline.

BAT mitochondrial respiration analysis—For the isolation of mitochondria from brown adipose tissue (Fischer et al., 2017; Shabalina et al., 2013), BATs of 4-5 mice were pooled in ice-cold 0.25 M sucrose. Tissues were minced, further homogenized in a glass homogenizer, filtered through a 250 μm nylon filter and centrifuged at 8500 g (JA-2550, Beckmann) for 10 min. The supernatant was discarded by inverting the tube, the pellet was resuspended in 0.25 M sucrose, homogenized in a glass homogenizer and centrifuged at 800 x g for 10 min. The supernatant, containing mitochondria, was centrifuged at 8500 x g for 10 min and the mitochondrial pellet was resuspended in TES buffer (100 mM KCl, 20 mM TES, 0.6% BSA, pH 7.2) to induce mitochondrial swelling. After centrifugation at 8500 g for 10 min, the supernatant was discarded, and the mitochondria were resuspended in remaining TES buffer. The solution was transferred to a small glass homogenizer, homogenized, and 0.4 mg of mitochondrial protein were used per measurement in the high-resolution respirometer ORO-BOROS Oxygraph-2k. The oxygen electrode chambers were filled with 2 mL preheated MiR-05 buffer (Oroboros Instruments, 110 mM sucrose, 60 mM K-lactobionate, 0.5 mM EGTA, 3 mM $MgCl_2$, 20 mM taurine, 10 mM KH_2PO_4, 20 mM HEPES, pH 7.1 and 0.1% fatty acid free BSA), magnetically stirred at 500 rpm and kept at 37°C. After introducing mitochondria to the chamber, oxygen consumption was measured in the presence of 2 mM malate (M), 12.5 mM pyruvate (P) and 10 mM L-glutamate (G) (all from Sigma). UCP1-dependent oxygen consumption was analyzed by titrating GDP to a final concentration of 5-6.25 mM. Subsequently, 1 mM ADP was added as a substrate for ATP synthase to measure maximal ADP-stimulated respiration. Thereafter the ATP synthase

was inhibited by 5 μM oligomycin. Eventually, maximal oxygen consumption was measured by titrating carbonyl cyanide m-chlorophenylhydrazine (CCCP) to a final concentration of 4-5 μM and residual oxygen consumption was measured adding 2.5 μM antimycin A. Data were collected and analyzed using DatLab 7. UCP1-activity was calculated as the difference between oxygen consumption in the presence of MPG and after addition of GDP. Maximal respiration was calculated as CCCP-induced respiration. Data were expressed as respiratory rates per BAT depot.

Immunohistochemistry—Immunohistochemistry was performed on paraffin embedded tissues. Sections were mounted on Superfrost Plus adhesion slides (Thermo), then deparaffinized and rehydrated as described above. Antigen retrieval was performed by boiling the slides in citrate buffer (10 mM sodium citrate, 0.05% Tween 20, pH 6) in a water bath for 30 min. The slides were cooled down to room temperature for 30 min. Slides were rinsed with PBS (GIBCO® DPBS) and incubated with blocking buffer (3% BSA in PBS) for 1 h at room temperature. All incubations were performed in a humidity chamber. The slides were incubated with the primary antibody (anti-UCP1, 1:1000) diluted in 1% BSA in PBS overnight at 4°C. After primary antibody incubation, the slides were washed with PBS for 3x 10 min and then incubated with goat-anti-rabbit HRP secondary antibody at a 1:500 dilution for 1 h at room temperature. After secondary antibody incubation, sections were washed with PBS for 3x 10 min. Staining was performed using abcam DAB kit following the manufacturer's instructions. After DAB-staining, the slides were rinsed with PBS to stop the chromogenic reaction and counterstained with hematoxilin for 2 min. Slides were incubated under running tap water for 10 min to achieve bluing of the hematoxilin. Afterward, the slides were dehydrated and mounted using Eukitt. Microscopy was performed on a Nikon A1 Microscope equipped with a DS-U3 camera (Nikon).

Imaging of endogenous and mWasabi-tagged LC3—For imaging of endogenous LC3 punctae, paraffin tissue sections from 30°C-acclimated mice were rehydrated and antigen retrieval was performed as for the immunohistochemical analysis. To reduce background, sections were incubated with 1% Sudan black (Sigma) in 80% ethanol for 10 min, and then washed in PBS. After blocking with 3% BSA (Sigma) in PBS for 1 h at room temperature, slides were incubated with anti-LC3B antibody (1:200) overnight at 4°C in a humid incubation chamber. After washing with PBS, sections were incubated with AF488-donkey-anti-rabbit secondary antibody (1:250) for 1 h at room temperature in the dark. Sections were then washed with PBS and stained with 0.05% DAPI in PBS for 10 min, before mounting with ProLong Gold antifade reagent.

For targeted expression of mWasabi-tagged LC3 in BAT, mice were injected with 5 mg/kg carprofen and anaesthetized with 4% isoflurane inhalation anesthesia in O_2. The interscapular region was shaved, sterilized with 80% ethanol, and the skin was opened in a 1 cm incision. BAT was carefully lifted up and 10 μl of AAV1 vectors containing an mWasabi-LC3 insert (concentration $5.1*10^{13}$ vg/ml) were injected into BAT using a 25 μl Hamilton syringe with a 30G needle. The skin incision was closed, animals received analgesia and antibiotics for recovery and were transferred to 30°C for one week. BAT was harvested and immediately imaged. Imaging was performed using a Nikon eclipse Ti confocal laser

scanning microscope with 488 nm laser and a 500–550 nm detector. LC3 punctae were counted in a blinded fashion and expressed per field.

Structural lipidomic analysis—Tissue samples were transferred to an Omni homogenizing tube with ceramic beads on ice. Tissue samples were homogenized in 0.1x PBS at 4°C for 1.5 minutes using an Omni Bead Ruptor with an attached Cryo unit. Sample aliquot volume was normalized by 1 mg protein determined by bicinchoninic acid (BCA) assay. Structural lipidomic analysis involved a modified Bligh and Dyer extraction utilizing a customized, automated liquid-liquid extraction sequence on a Hamilton Robotics Star^{LET} Robot System. Four mL of chloroform:methanol (1:1, by vol) was added to the samples followed by addition of 50 μL of a cocktail mixture of deuterium-labeled, odd chain, and extremely low naturally abundant internal standards. A front extraction was performed by adding 2 mL of 50mM lithium chloride to sample tubes, vortexed in Multi Tube Vortexer for 3 minutes, centrifuged at 1000 *g* for five minutes, and the bottom chloroform layer was carefully transferred to a new glass tube. An additional 1.8 mL of chloroform was added to source tubes, vortexed and centrifuged as described above, and transferred for a total of three chloroform transfers. The samples were dried down under a stream of N_2 gas and resuspended in chloroform:methanol (1:1, by vol). A back extraction was performed for additional sample clean up to remove contamination of protein, salts, and residual aqueous layer from front extraction. Two mL of 10mM lithium chloride was added to resuspended samples and same protocol was followed as front extraction. Samples were dried down under N_2, reconstituted in chloroform:methanol (1:1, by vol), and stored at −20°C. Samples were prepared to run on the mass spectrometer by diluting 250x in isopropanol:methanol:acetonitrile:water (3:3:3:1, by vol) with 2 mM ammonium acetate.

Electrospray ionization (ESI) MS was performed on a Sciex TripleTOF 5600+ coupled with a direct injection loop on an Eksigent Ekspert MicroLC 200 system. The ESI DuoSpray Ion Source parameter settings were set to: ion source gas 1 (GS1) at 10, ion source gas 2 (GS2) at 10, curtain gas (CUR) at 20, temperature at 300°C, and Ion Spray Voltage Floating (ISVF) at 5500 V for positive mode and −4500 V for negative mode. The MS/MS^{ALL} acquisition method consisted of two experiments, first a TOF MS survey scan acquiring data from 200-1200 m/z. The second experiment in the acquisition method consisted of 1000 high resolution product ion scans with precursors evenly spaced from m/z 200.05 to m/z 1200.05 with 300 ms of accumulation time for each scan. The collision energy was set to 35 eV and −35 eV for positive and negative mode, respectively, with a collision energy spread (CES) of ± 15 eV. Cardiolipin and monoacylglycerol species were analyzed with unique acquisition methods as previously described (Gao et al., 2016, 2018). Mass shift was controlled by calibrant solution delivered every 10 samples at 500 μL/min by the atmospheric-pressure chemical ionization (APCI) probe. The MS/MS^{ALL} data was acquired by Analyst TF 1.7 software (Sciex) and processed with MultiQuant 1.2.2.5 (Sciex) using an in-house database of lipid species for identification and quantification.

Fatty acid profiling—Fatty acid composition in total lipid extracts of tissues was determined by gas chromatography, as described previously (Scheja et al., 2008). Briefly, 250 μL of butylhydroxytoluene (0.1 mol l–1 in methanol) and 6 mL of chloroform/methanol

(2/1, v/v) were added to ~50-100 mg of tissue. After homogenization using an Ultraturrax homogenizer, the samples were heated to 50°C for 30 min and centrifuged (1,800 g, 5 min). Fatty acid methyl esters were prepared by heating 100 μL of tissue extract, 2 mL methanol/toluene (4/1, v/v), 50 μL heptadecanoic acid (200 mg ml–1 in methanol/toluene, 4/1) and 200 μL acetyl chloride in a capped tube for 1 h at 100°C. After cooling to room temperature, 5 mL of 6% sodium carbonate and 1.6 mL of toluene were added. The mixture was centrifuged (1,800 g, 5 min) and 150–200 μL of the upper layer was transferred to auto sampler vials. Gas chromatography analyses were performed using an HP 5890 gas chromatograph (Hewlett Packard) equipped with flame ionization detectors (Stationary phase: DB-225 30 m × 0.25 mm i.d., film thickness 0.25 μm; Agilent). Peak identification and quantification were performed by comparing retention times and peak areas, respectively, to standard chromatograms. All calculations are based on fatty acid methyl ester values.

Human BAT sampling—Brown adipose tissue biopsies were obtained from the supraclavicular deep neck of 31 patients undergoing thyroid surgery due to benign goiter. Biopsies were immediately snap frozen in liquid nitrogen and stored at −80°C until RNA isolation.

QUANTIFICATION AND STATISTICAL ANALYSIS

Two groups were compared by unpaired two-tailed Student's t test, more than two groups by two-way ANOVA. Statistical analyses were conducted using Graph Pad software; $p < 0.05$ was considered significant. The numbers of animals per group (n) and the exact statistical tests used can be found in the figure legends.

Supplementary Material

Refer to Web version on PubMed Central for supplementary material.

ACKNOWLEDGMENTS

L.S. and J.H. were supported by the Deutsche Forschungsgemeinschaft (SCHE522/4-1 and HE3645/10-1). C. Schlein was supported by a fellowship from the Gertraud and Heinz Rose Foundation, the Christine-Katharina-Schmitz-Foundation, and the UKE MD/PhD program fellowship. A.W.F. was supported by the German National Academic Foundation, a DFG postdoctoral fellowship (FI2476/1-1), and a project grant by the DACH Gesellschaft für Lipidologie. A.B. was supported by the Deutsche Forschungsgemeinschaft Son-derforschungsbereich 1123 (B10), and a Deutsches Zentrum für Herz-Kreislauf-Forschung Junior Research Group grant. N.Z.J. was supported by an individual research grant from the Danish Diabetes Academy funded by the Novo Nordisk Foundation (NNF17SA0031406). The Centre for Physical Activity Research is supported by TrygFonden (grants ID 101390 and ID 20045). Visualization graphics were created using Biorender.com. The authors thank Sandra Ehret, Eva-Marie Azizi, Birgit Henkel, Meike Kröger, Anastasia Kuhl, Judith Schreiber, and Paul Pertzborn for excellent technical assistance.

REFERENCES

Abdul-Wahed A, Guilmeau S, and Postic C (2017). Sweet Sixteenth for ChREBP: Established Roles and Future Goals. Cell Metab. 26, 324–341. [PubMed: 28768172]

Adlanmerini M, Carpenter BJ, Remsberg JR, Aubert Y, Peed LC, Richter HJ, and Lazar MA (2019). Circadian lipid synthesis in brown fat maintains murine body temperature during chronic cold. Proc. Natl. Acad. Sci. USA 116, 18691–18699. [PubMed: 31451658]

Altshuler-Keylin S, Shinoda K, Hasegawa Y, Ikeda K, Hong H, Kang Q, Yang Y, Perera RM, Debnath J, and Kajimura S (2016). Beige Adipocyte Maintenance Is Regulated by Autophagy-Induced Mitochondrial Clearance. Cell Metab. 24, 402–419. [PubMed: 27568548]

Bartelt A, and Heeren J (2012). The holy grail of metabolic disease: brown adipose tissue. Curr. Opin. Lipidol 23, 190–195. [PubMed: 22449813]

Bartelt A, Bruns OT, Reimer R, Hohenberg H, Ittrich H, Peldschus K, Kaul MG, Tromsdorf UI, Weller H, Waurisch C, et al. (2011). Brown adipose tissue activity controls triglyceride clearance. Nat. Med 17, 200–205. [PubMed: 21258337]

Bartelt A, Widenmaier SB, Schlein C, Johann K, Goncalves RLS, Eguchi K, Fischer AW, Parlakgül G, Snyder NA, Nguyen TB, et al. (2018). Brown adipose tissue thermogenic adaptation requires Nrf1-mediated proteasomal activity. Nat. Med 24, 292–303. [PubMed: 29400713]

Blommaart EF, Krause U, Schellens JP, Vreeling-Sindelárová H, and Meijer AJ (1997). The phosphatidylinositol 3-kinase inhibitors wortmannin and LY294002 inhibit autophagy in isolated rat hepatocytes. Eur. J. Biochem 243, 240–246. [PubMed: 9030745]

Cannon B, and Nedergaard J (2004). Brown adipose tissue: function and physiological significance. Physiol. Rev 84, 277–359. [PubMed: 14715917]

Cannon B, de Jong JMA, Fischer AW, Nedergaard J, and Petrovic N (2020). Human brown adipose tissue: Classical brown rather than brite/beige? Exp. Physiol 105, 1191–1200. [PubMed: 32378255]

Chen KY, Brychta RJ, Abdul Sater Z, Cassimatis TM, Cero C, Fletcher LA, Israni NS, Johnson JW, Lea HJ, Linderman JD, et al. (2020). Opportunities and challenges in the therapeutic activation of human energy expenditure and thermogenesis to manage obesity. J. Biol. Chem 295, 1926–1942. [PubMed: 31914415]

Chu CT, Ji J, Dagda RK, Jiang JF, Tyurina YY, Kapralov AA, Tyurin VA, Yanamala N, Shrivastava IH, Mohammadyani D, et al. (2013). Cardiolipin externalization to the outer mitochondrial membrane acts as an elimination signal for mitophagy in neuronal cells. Nat. Cell Biol 15, 1197–1205. [PubMed: 24036476]

Cypess AM, Lehman S, Williams G, Tal I, Rodman D, Goldfine AB, Kuo FC, Palmer EL, Tseng YH, Doria A, et al. (2009). Identification and importance of brown adipose tissue in adult humans. N. Engl. J. Med 360, 1509–1517. [PubMed: 19357406]

Cypess AM, Weiner LS, Roberts-Toler C, Franquet Elía E, Kessler SH, Kahn PA, English J, Chatman K, Trauger SA, Doria A, and Kolodny GM (2015). Activation of human brown adipose tissue by a β3-adrenergic receptor agonist. Cell Metab. 21, 33–38. [PubMed: 25565203]

de Jong JMA, Sun W, Pires ND, Frontini A, Balaz M, Jespersen NZ, Feizi A, Petrovic K, Fischer AW, Bokhari MH, et al. (2019). Human brown adipose tissue is phenocopied by classical brown adipose tissue in physiologically humanized mice. Nat. Metab 1, 830–843. [PubMed: 32694768]

Eissing L, Scherer T, Tödter K, Knippschild U, Greve JW, Buurman WA, Pinnschmidt HO, Rensen SS, Wolf AM, Bartelt A, et al. (2013). De novo lipogenesis in human fat and liver is linked to ChREBP-β and metabolic health. Nat. Commun 4, 1528. [PubMed: 23443556]

Epand RM (1998). Lipid polymorphism and protein-lipid interactions. Biochim. Biophys. Acta 1376, 353–368.

Fajardo VA, Mikhaeil JS, Leveille CF, Saint C, and LeBlanc PJ (2017). Cardiolipin content, linoleic acid composition, and tafazzin expression in response to skeletal muscle overload and unload stimuli. Sci. Rep 7, 2060. [PubMed: 28515468]

Feldmann HM, Golozoubova V, Cannon B, and Nedergaard J (2009). UCP1 ablation induces obesity and abolishes diet-induced thermogenesis in mice exempt from thermal stress by living at thermoneutrality. Cell Metab. 9, 203–209. [PubMed: 19187776]

Fischer AW, Shabalina IG, Mattsson CL, Abreu-Vieira G, Cannon B, Nedergaard J, and Petrovic N (2017). UCP1 inhibition in Cidea-overexpressing mice is physiologically counteracted by brown adipose tissue hyperrecruitment. Am. J. Physiol. Endocrinol. Metab 312, E72–E87. [PubMed: 27923808]

Fischer AW, Cannon B, and Nedergaard J (2018). Optimal housing temperatures for mice to mimic the thermal environment of humans: An experimental study. Mol. Metab 7, 161–170. [PubMed: 29122558]

Fischer AW, Cannon B, and Nedergaard J (2019a). The answer to the question “What is the best housing temperature to translate mouse experiments to humans?” is: thermoneutrality. Mol. Metab 26, 1–3. [PubMed: 31155502]

Fischer AW, Schlein C, Cannon B, Heeren J, and Nedergaard J (2019b). Intact innervation is essential for diet-induced recruitment of brown adipose tissue. Am. J. Physiol. Endocrinol. Metab 316, E487–E503. [PubMed: 30576247]

Ganeshan K, and Chawla A (2017). Warming the mouse to model human diseases. Nat. Rev. Endocrinol 13, 458–465. [PubMed: 28497813]

Gao F, McDaniel J, Chen EY, Rockwell H, Lynes MD, Tseng YH, Sarangarajan R, Narain NR, and Kiebish MA (2016). Monoacylglycerol Analysis Using MS/MS(ALL) Quadruple Time of Flight Mass Spectrometry. Metabolites 6, 25.

Gao F, McDaniel J, Chen EY, Rockwell HE, Nguyen C, Lynes MD, Tseng YH, Sarangarajan R, Narain NR, and Kiebish MA (2018). Adapted MS/MS^{ALL} Shotgun Lipidomics Approach for Analysis of Cardiolipin Molecular Species. Lipids 53, 133–142. [PubMed: 29488636]

Gross AS, Zimmermann A, Pendl T, Schroeder S, Schoenlechner H, Knittelfelder O, Lamplmayr L, Santiso A, Aufschnaiter A, Waltenstorfer D, et al. (2019). Acetyl-CoA carboxylase 1-dependent lipogenesis promotes autophagy downstream of AMPK. J. Biol. Chem 294, 12020–12039. [PubMed: 31209110]

Han X, Yang J, Yang K, Zhao Z, Abendschein DR, and Gross RW (2007). Alterations in myocardial cardiolipin content and composition occur at the very earliest stages of diabetes: a shotgun lipidomics study. Biochemistry 46, 6417–6428. [PubMed: 17487985]

Hany TF, Gharehpapagh E, Kamel EM, Buck A, Himms-Hagen J, and von Schulthess GK (2002). Brown adipose tissue: a factor to consider in symmetrical tracer uptake in the neck and upper chest region. Eur. J. Nucl. Med. Mol. Imaging 29, 1393–1398. [PubMed: 12271425]

Harwood HJ Jr., Petras SF, Shelly LD, Zaccaro LM, Perry DA, Makowski MR, Hargrove DM, Martin KA, Tracey WR, Chapman JG, et al. (2003). Isozyme-nonselective N-substituted bipiperidylcarboxamide acetyl-CoA carboxylase inhibitors reduce tissue malonyl-CoA concentrations, inhibit fatty acid synthesis, and increase fatty acid oxidation in cultured cells and in experimental animals. J. Biol. Chem 278, 37099–37111. [PubMed: 12842871]

Heine M, Fischer AW, Schlein C, Jung C, Straub LG, Gottschling K, Mangels N, Yuan Y, Nilsson SK, Liebscher G, et al. (2018). Lipolysis Triggers a Systemic Insulin Response Essential for Efficient Energy Replenishment of Activated Brown Adipose Tissue in Mice. Cell Metab. 28, 644–655.e4. [PubMed: 30033199]

Herman MA, Peroni OD, Villoria J, Schön MR, Abumrad NA, Blüher M, Klein S, and Kahn BB (2012). A novel ChREBP isoform in adipose tissue regulates systemic glucose metabolism. Nature 484, 333–338. [PubMed: 22466288]

Hsu P, Liu X, Zhang J, Wang HG, Ye JM, and Shi Y (2015). Cardiolipin remodeling by TAZ/tafazzin is selectively required for the initiation of mitophagy. Autophagy 11, 643–652. [PubMed: 25919711]

Iizuka K, Bruick RK, Liang G, Horton JD, and Uyeda K (2004). Deficiency of carbohydrate response element-binding protein (ChREBP) reduces lipogenesis as well as glycolysis. Proc. Natl. Acad. Sci. USA 101, 7281–7286. [PubMed: 15118080]

Janikiewicz J, Hanzelka K, Dziewulska A, Kozinski K, Dobrzyn P, Bernas T, and Dobrzyn A (2015). Inhibition of SCD1 impairs palmitate-derived autophagy at the step of autophagosome-lysosome fusion in pancreatic β-cells. J. Lipid Res 56, 1901–1911. [PubMed: 26293158]

Jeon TI, and Osborne TF (2012). SREBPs: metabolic integrators in physiology and metabolism. Trends Endocrinol. Metab 23, 65–72. [PubMed: 22154484]

Jespersen NZ, Andersen MW, Jensen VH, Stærkær TW, Severinsen MCK, Peijs L, Soares R, Forss I, Andersen ES, Hahn CH, et al. (2020). Thermogenic genes are blunted whereas brown adipose tissue identity is preserved in human obesity. bioRxiv. 10.1101/2020.05.07.082057.

Jois T, Chen W, Howard V, Harvey R, Youngs K, Thalmann C, Saha P, Chan L, Cowley MA, and Sleeman MW (2017). Deletion of hepatic carbohydrate response element binding protein (ChREBP) impairs glucose homeostasis and hepatic insulin sensitivity in mice. Mol. Metab 6, 1381–1394. [PubMed: 29107286]

Klionsky DJ (2011). For the last time, it is GFP-Atg8, not Atg8-GFP (and the same goes for LC3). Autophagy 7, 1093–1094. [PubMed: 21993240]

Koenig BW, Strey HH, and Gawrisch K (1997). Membrane lateral compressibility determined by NMR and x-ray diffraction: effect of acyl chain polyunsaturation. Biophys. J 73, 1954–1966. [PubMed: 9336191]

Komiya K, Uchida T, Ueno T, Koike M, Abe H, Hirose T, Kawamori R, Uchiyama Y, Kominami E, Fujitani Y, and Watada H (2010). Free fatty acids stimulate autophagy in pancreatic β-cells via JNK pathway. Biochem. Biophys. Res. Commun 401, 561–567. [PubMed: 20888798]

Lee HJ, Mayette J, Rapoport SI, and Bazinet RP (2006). Selective remodeling of cardiolipin fatty acids in the aged rat heart. Lipids Health Dis. 5, 2. [PubMed: 16430781]

Li Y, Schnabl K, Gabler S-M, Willershäuser M, Reber J, Karlas A, Laurila S, Lahesmaa M, Din MU, Bast-Habersbrunner A, et al. (2018). Secretin-Activated Brown Fat Mediates Prandial Thermogenesis to Induce Satiation. Cell 175, 1561–1574.e12. [PubMed: 30449620]

Lu X, Altshuler-Keylin S, Wang Q, Chen Y, Henrique Sponton C, Ikeda K, Maretich P, Yoneshiro T, and Kajimura S (2018). Mitophagy controls beige adipocyte maintenance through a Parkin-dependent and UCP1-independent mechanism. Sci. Signal 11, eaap8526. [PubMed: 29692364]

Mottillo EP, Balasubramanian P, Lee YH, Weng C, Kershaw EE, and Granneman JG (2014). Coupling of lipolysis and de novo lipogenesis in brown, beige, and white adipose tissues during chronic β3-adrenergic receptor activation. J. Lipid Res 55, 2276–2286. [PubMed: 25193997]

Nedergaard J, Bengtsson T, and Cannon B (2007). Unexpected evidence for active brown adipose tissue in adult humans. Am. J. Physiol. Endocrinol. Metab 293, E444–E452. [PubMed: 17473055]

O'Mara AE, Johnson JW, Linderman JD, Brychta RJ, McGehee S, Fletcher LA, Fink YA, Kapuria D, Cassimatis TM, Kelsey N, et al. (2020). Chronic mirabegron treatment increases human brown fat, HDL cholesterol, and insulin sensitivity. J. Clin. Invest 130, 2209–2219. [PubMed: 31961826]

Rosenwald M, Perdikari A, Rülicke T, and Wolfrum C (2013). Bi-directional interconversion of brite and white adipocytes. Nat. Cell Biol 15, 659–667. [PubMed: 23624403]

Saini-Chohan HK, Holmes MG, Chicco AJ, Taylor WA, Moore RL, McCune SA, Hickson-Bick DL, Hatch GM, and Sparagna GC (2009). Cardiolipin biosynthesis and remodeling enzymes are altered during development of heart failure. J. Lipid Res 50, 1600–1608. [PubMed: 19001357]

Saini-Chohan HK, Dakshinamurti S, Taylor WA, Shen GX, Murphy R, Sparagna GC, and Hatch GM (2011). Persistent pulmonary hypertension results in reduced tetralinoleoyl-cardiolipin and mitochondrial complex II + III during the development of right ventricular hypertrophy in the neonatal pig heart. Am. J. Physiol. Heart Circ. Physiol 301, H1415–H1424. [PubMed: 21841017]

Saito M, Okamatsu-Ogura Y, Matsushita M, Watanabe K, Yoneshiro T, Nio-Kobayashi J, Iwanaga T, Miyagawa M, Kameya T, Nakada K, et al. (2009). High incidence of metabolically active brown adipose tissue in healthy adult humans: effects of cold exposure and adiposity. Diabetes 58, 1526–1531. [PubMed: 19401428]

Sanchez-Gurmaches J, Tang Y, Jespersen NZ, Wallace M, Martinez Calejman C, Gujja S, Li H, Edwards YJK, Wolfrum C, Metallo CM, et al. (2018). Brown Fat AKT2 Is a Cold-Induced Kinase that Stimulates ChREBP-Mediated De Novo Lipogenesis to Optimize Fuel Storage and Thermogenesis. Cell Metab. 27, 195–209.e6. [PubMed: 29153407]

Scheele C, and Wolfrum C (2020). Brown Adipose Crosstalk in Tissue Plasticity and Human Metabolism. Endocr. Rev 41, 53–65.

Scheja L, Toedter K, Mohr R, Niederfellner G, Michael MD, Meissner A, Schoettler A, Pospisil H, Beisiegel U, and Heeren J (2008). Liver TAG transiently decreases while PL n-3 and n-6 fatty acids are persistently elevated in insulin resistant mice. Lipids 43, 1039–1051. [PubMed: 18763007]

Schenkel LC, and Bakovic M (2014). Formation and regulation of mitochondrial membranes. Int. J. Cell Biol 2014, 709828. [PubMed: 24578708]

Schlein C, and Heeren J (2016). Implications of thermogenic adipose tissues for metabolic health. Best Pract. Res. Clin. Endocrinol. Metab 30, 487–496. [PubMed: 27697210]

Schütter M, Giavalisco P, Brodesser S, and Graef M (2020). Local Fatty Acid Channeling into Phospholipid Synthesis Drives Phagophore Expansion during Autophagy. Cell 180, 135–149.e14. [PubMed: 31883797]

Shabalina IG, Petrovic N, de Jong JM, Kalinovich AV, Cannon B, and Nedergaard J (2013). UCP1 in brite/beige adipose tissue mitochondria is functionally thermogenic. Cell Rep. 5, 1196–1203. [PubMed: 24290753]

Shimano H, and Sato R (2017). SREBP-regulated lipid metabolism: convergent physiology–divergent pathophysiology. Nat. Rev. Endocrinol 13, 710–730. [PubMed: 28849786]

Škop V, Guo J, Liu N, Xiao C, Hall KD, Gavrilova O, and Reitman ML (2020). Mouse Thermoregulation: Introducing the Concept of the Thermoneutral Point. Cell Rep. 31, 107501. [PubMed: 32294435]

Smaby JM, Momsen MM, Brockman HL, and Brown RE (1997). Phosphatidylcholine acyl unsaturation modulates the decrease in interfacial elasticity induced by cholesterol. Biophys. J 73, 1492–1505. [PubMed: 9284316]

Sparagna GC, Chicco AJ, Murphy RC, Bristow MR, Johnson CA, Rees ML, Maxey ML, McCune SA, and Moore RL (2007). Loss of cardiac tetralinoleoyl cardiolipin in human and experimental heart failure. J. Lipid Res 48, 1559–1570. [PubMed: 17426348]

Stanley WC, Khairallah RJ, and Dabkowski ER (2012). Update on lipids and mitochondrial function: impact of dietary n-3 polyunsaturated fatty acids. Curr. Opin. Clin. Nutr. Metab. Care 15, 122–126. [PubMed: 22248591]

Sullivan EM, Pennington ER, Green WD, Beck MA, Brown DA, and Shaikh SR (2018). Mechanisms by Which Dietary Fatty Acids Regulate Mitochondrial Structure-Function in Health and Disease. Adv. Nutr 9, 247–262. [PubMed: 29767698]

Trayhurn P (1981). Fatty acid synthesis in mouse brown adipose tissue. The influence of environmental temperature on the proportion of whole-body fatty acid synthesis in brown adipose tissue and the liver. Biochim. Biophys. Acta 664, 549–560. [PubMed: 7272321]

van der Lans AA, Hoeks J, Brans B, Vijgen GH, Visser MG, Vosselman MJ, Hansen J, Jörgensen JA, Wu J, Mottaghy FM, et al. (2013). Cold acclimation recruits human brown fat and increases nonshivering thermogenesis. J. Clin. Invest 123, 3395–3403. [PubMed: 23867626]

van Marken Lichtenbelt WD, Vanhommerig JW, Smulders NM, Drossaerts JM, Kemerink GJ, Bouvy ND, Schrauwen P, and Teule GJ (2009). Cold-activated brown adipose tissue in healthy men. N. Engl. J. Med 360, 1500–1508. [PubMed: 19357405]

Vijayakumar A,Aryal P,Wen J, Syed I,Vazirani RP, Moraes-Vieira PM, Camporez JP, Gallop MR, Perry RJ, Peroni OD, et al. (2017). Absence of Carbohydrate Response Element Binding Protein in Adipocytes Causes Systemic Insulin Resistance and Impairs Glucose Transport. Cell Rep. 21, 1021–1035. [PubMed: 29069585]

Virtanen KA, Lidell ME, Orava J, Heglind M, Westergren R, Niemi T, Taittonen M, Laine J, Savisto NJ, Enerbäck S, and Nuutila P (2009). Functional brown adipose tissue in healthy adults. N. Engl. J. Med 360, 1518–1525. [PubMed: 19357407]

von Essen G, Lindsund E, Cannon B, and Nedergaard J (2017). Adaptive facultative diet-induced thermogenesis in wild-type but not in UCP1-ablated mice. Am. J. Physiol. Endocrinol. Metab 313, E515–E527. [PubMed: 28679625]

Wang Y, Viscarra J, Kim SJ, and Sul HS (2015). Transcriptional regulation of hepatic lipogenesis. Nat. Rev. Mol. Cell Biol 16, 678–689. [PubMed: 26490400]

Wei C, Ma X, Su K, Qi S, Zhu Y, Lin J, Wang C, Yang R, Chen X, Wang W, and Zhang WJ (2020). ChREBP-β regulates thermogenesis in brown adipose tissue. J. Endocrinol 245, 343–356. [PubMed: 32208359]

Yang YP, Hu LF, Zheng HF, Mao CJ, Hu WD, Xiong KP, Wang F, and Liu CF (2013). Application and interpretation of current autophagy inhibitors and activators. Acta Pharmacol. Sin 34, 625–635. [PubMed: 23524572]

Zingaretti MC, Crosta F, Vitali A, Guerrieri M, Frontini A, Cannon B, Nedergaard J, and Cinti S (2009). The presence of UCP1 demonstrates that metabolically active adipose tissue in the neck of adult humans truly represents brown adipose tissue. FASEB J. 23, 3113–3120. [PubMed: 19417078]

Highlights

- ChREBP controls de *novo* lipogenesis (DNL) in BAT
- DNL-derived lipids are enriched in BAT of mice in response to thermoneutral housing
- Thermoneutrality causes loss of mitochondria and UCP1 by mitophagy in BAT
- DNL-linked lipid remodeling and BAT involution are prevented by ChREBP deficiency

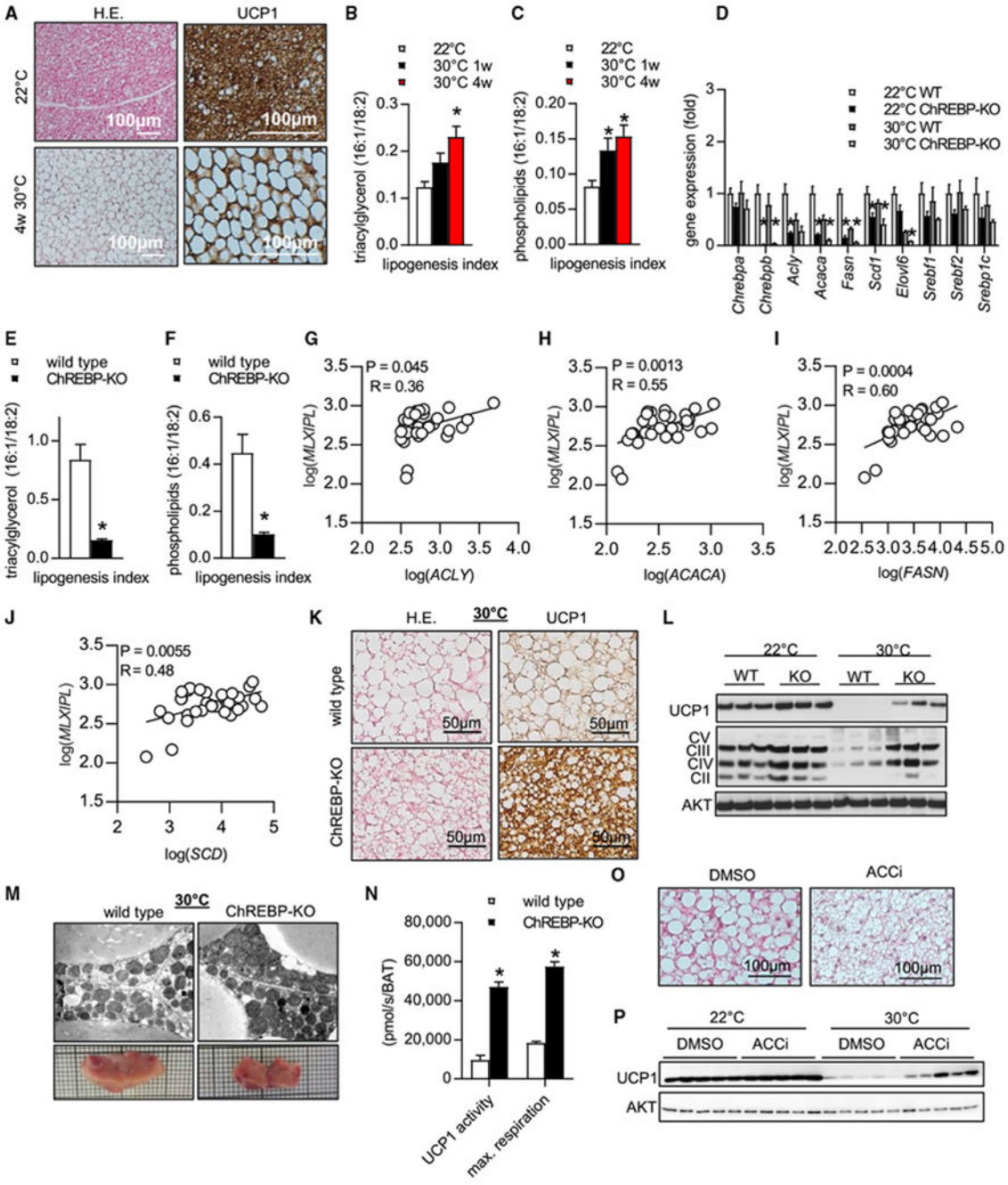

Figure 1. Fatty Acid Synthesis Is Essential for BAT Whitening

BAT was harvested from wild-type mice or mice with genetic or pharmacological inhibition of lipogenesis, housed at room temperature (22°C) or adapted to thermoneutrality (30°C) for the time periods indicated.

(A–C) Wild-type mice.

(A) Representative images of hematoxylin and eosin (H&E) and UCP1 immunohistochemistry stainings (n = 5).

(B) The ratio of palmitoleate to linoleate (lipogenesis index) in triacylglycerols (n = 6).

(C) Lipogenesis index in phospholipids (n = 6).
(D–F) Wild-type and ChREBP-KO mice.
(D) Expression of lipogenic genes in thermoneutral BAT of mice housed at room temperature or at thermoneutrality for 6 weeks (n = 6).
(E and F) Lipogenesis index in triacylglycerols (E) and phospholipids (F) in thermoneutral BAT following 12-week adaptation to thermoneutrality (n = 6).
(G–J) RNA-seq gene expression analysis of human BAT (n = 31).
(G) Correlation of *MLXIPL* with *ACLY.*
(H) Correlation of *MLXIPL* with *ACACA.*
(I) Correlation of *MLXIPL* with *FASN.*
(J) Correlation of *MLXIPL* with *SCD.*
(K–N) Wild-type and ChREBP-KO mice.
(K) Representative histological images and UCP1 immunostaining in BAT of mice housed for 6 weeks at thermoneutrality (n = 3).
(L) Western blot analysis of mitochondrial markers in BAT (n = 3).
(M) Representative BAT images and EM from mice housed for 12 weeks at thermoneutrality.
(N) UCP1-dependent and maximum respiration of mitochondria isolated from 1-week thermoneutral BAT (n = 3).
(O and P) Wild-type mice housed at 22°C or 30°C were injected with vehicle or ACC inhibitor.
(O) Representative images of H&E staining (n = 5).
(P) Western blot analysis of UCP1 and AKT (housekeeper) (n = 5).
Data are presented as means ± SEM. *$p < 0.05$ by Student's t test or one-way ANOVA.
See also Figure S1.

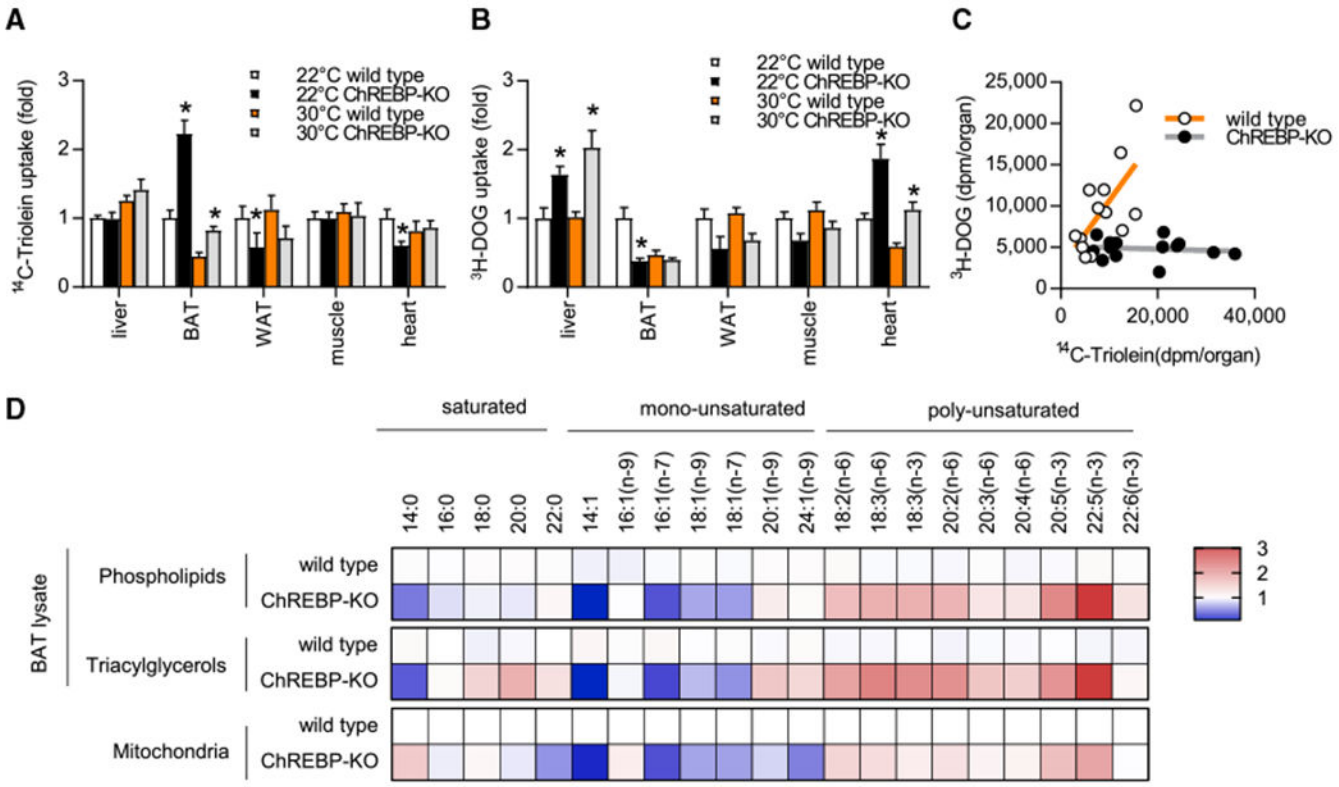

Figure 2. Reduced Endogenous Lipid Level of Triacylglycerols and Phospholipids in ChREBP-KO Mice Cannot Be Compensated by Dietary Lipids

Wild-type mice or ChREBP-KO mice were housed at room temperature (22°C) or adapted to thermoneutrality (30°C) for 1 week, and nutrient uptake and BAT fatty acid composition were determined.

(A) ^{14}C-triolein uptake in metabolically active organs (n = 6–7).

(B) ^{3}H-deoxyglucose (^{3}H-DOG) uptake in the same mice as in (A).

(C) Correlation of ^{14}C-triolein and ^{3}H-DOG uptake presented in (A) and (B).

(D) Fold changes in fatty acids in triacylglycerols, phospholipids, and mitochondrial lipid extracts from BAT of mice housed at 30°C (n = 6).

Data are presented as means ± SEM. *p < 0.05 by two-way ANOVA.

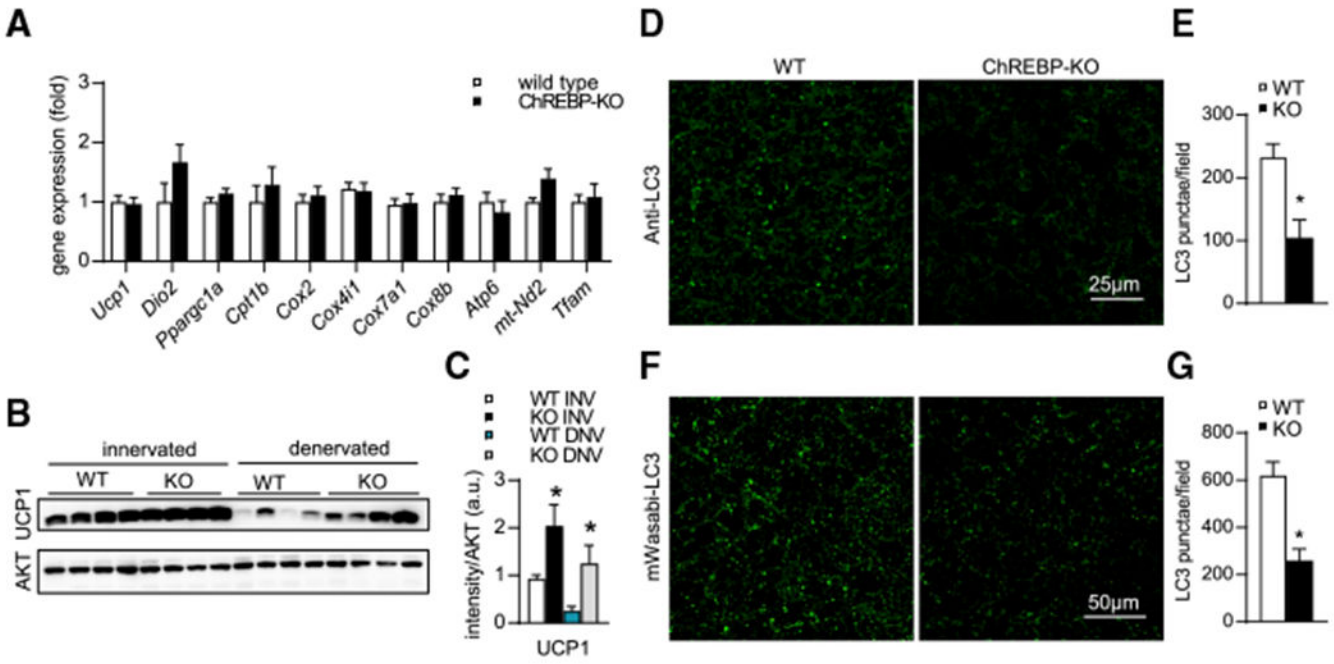

Figure 3. Loss of Endogenous Lipid Production Leads to Diminished Organelle Degradation

Wild-type and ChREBP-KO mice were housed at thermoneutrality for 1 week, housed at thermoneutrality for 1 week after injection of adeno-associated virus (AAV) encoding Wasabi-LC3, or housed at room temperature after BAT denervation.

(A) Expression of thermogenic genes in BAT after thermoneutral adaption for 1 week (n = 6).

(B) Western blot analysis of UCP1 and AKT in BAT of denervated or sham-treated mice (n = 4).

(C) Quantification of the western blot shown in (B) (n = 4).

(D and E) Immunostaining and quantification of LC3 punctae in BAT of overnight-fasted mice (n = 4–5).

(F and G) Samples of thermoneutral BAT were prepared for immunofluorescence after infection with an AAV construct encoding mWasabi-LC3 (n = 3).

Data are presented as means ± SEM. *p < 0.05 by Student's t test.

See also Figure S2.

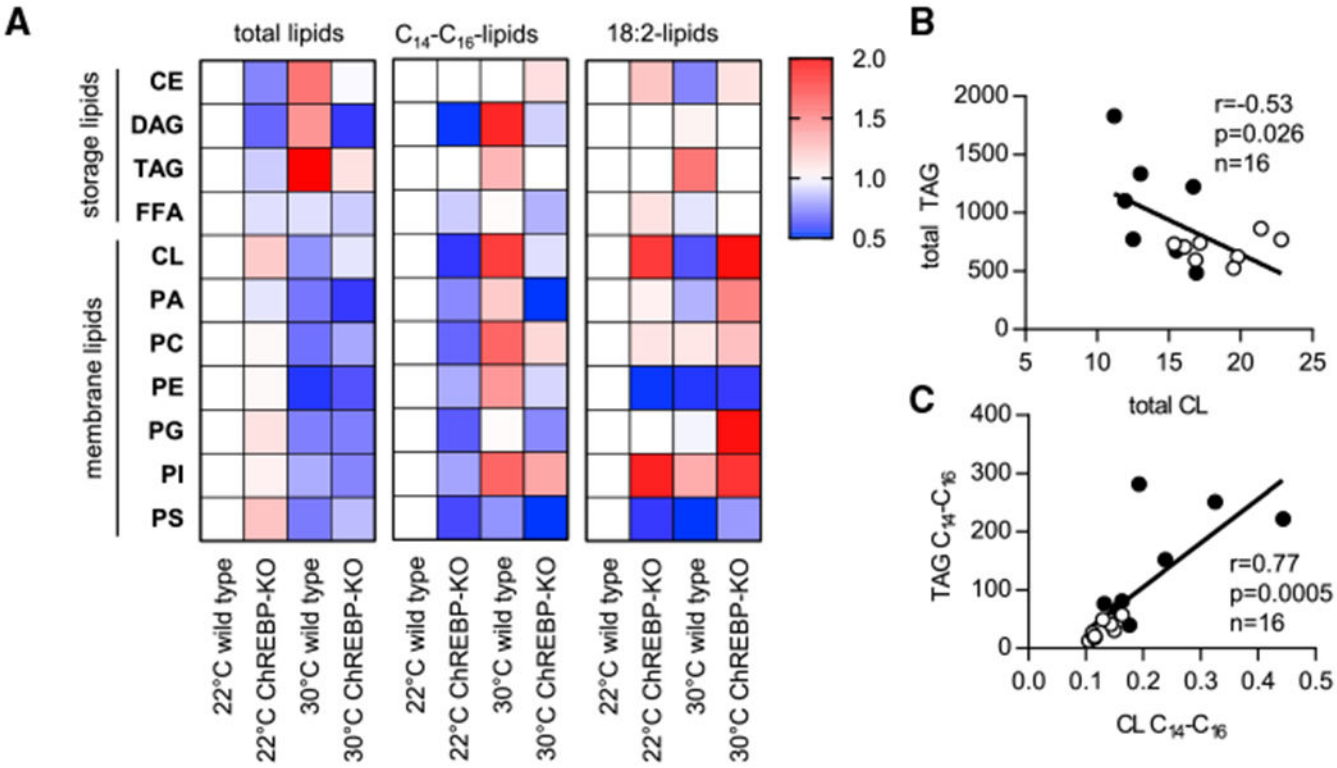

Figure 4. Lipogenesis Is Required for Remodeling of Membrane and Storage Lipids at Thermoneutrality

To elucidate which lipid classes were specifically affected by fatty acid remodeling during BAT whitening, lipidomic analysis of BAT from wild-type and ChREBP-KO mice acclimated to 22°C or 30°C was performed.

(A) Total lipid content of BAT (normalized on protein content), as well as enrichment of lipids containing endogenously produced C_{14}-C_{16} or diet-derived 18:2 fatty acids in different lipid classes of BAT. Data are means of n = 4 per group. Fold changes over levels in wild-type mice at 22°C are shown.

(B) Correlation between total cardiolipin and total triacylglycerol content in wild-type (black dots) and ChREBP-KO mice (white dots).

(C) Correlation between C14-C16-enriched cardiolipin and triacylglycerol levels in wild-type (black dots) and ChREBP-KO mice (white dots). CE, cholesterol ester; CL, cardiolipin; DAG, diacylglycerol; FFA, free fatty acid; PA, phosphatidic acid; PC, phosphatidylcholine; PE, phosphatidylethanolamine; PG, phosphatidylglycerol; PI; phosphatidylinositol; PS, phosphatidylserine; TAG, triacylglycerol.

See also Figure S3.

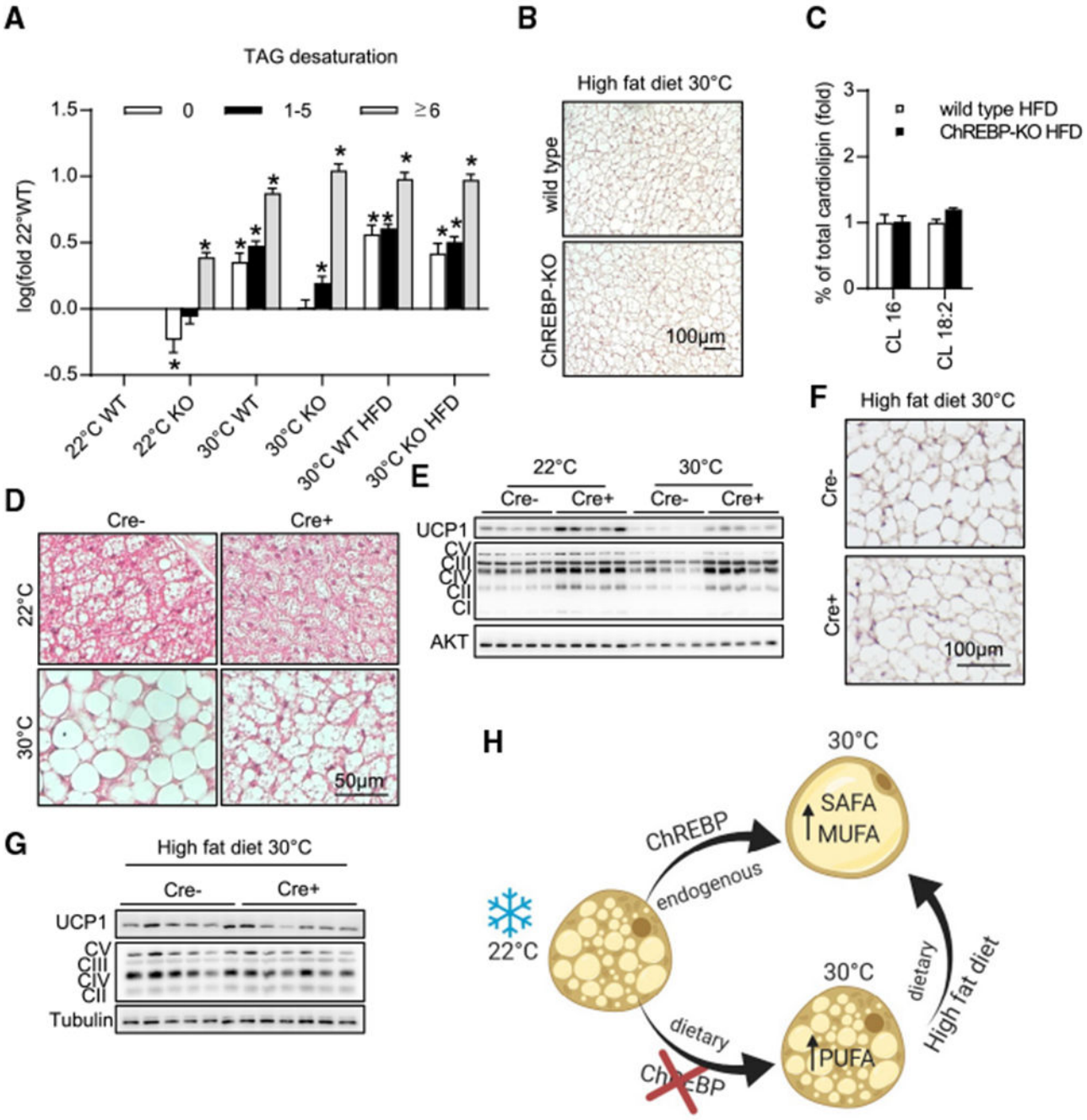

Figure 5. Excess Dietary Lipids Disconnect Lipid Storage from Mitochondrial Breakdown

Mice lacking ChREBP globally (ChREBP-KO) or specifically in thermogenic adipocytes (Cre^{+}) and littermate controls (wild-type/Cre^{-}) were housed at room temperature (22°C) and/or adapted to thermoneutrality (30°C) on chow diet or high-fat diet (HFD).

(A–C) Wild-type and ChREBP-KO mice.

(A) BAT triacylglycerol desaturation in mice fed either chow diet or HFD housed at indicated temperatures. Levels of triacylglycerols containing fatty acids with 0, 1–5, or ≥6 double bonds are shown. Log fold change over wild-type levels at 22°C are plotted (n = 4).

(B) Representative H&E staining of BAT in mice fed HFD at thermoneutrality (n = 6).
(C) Levels of cardiolipins enriched in C16 or C18:2 fatty acids (n = 4).
(D–G) Brown adipocyte-specific ChREBP-deficient (Cre^+) and control (Cre^-) mice.
(D) Representative BAT H&E staining of chow-fed mice (n = 5).
(E) Western blot analysis of UCP1 and OXPHOS complexes (CI-V) in chow-fed mice (n = 5).
(F) Representative H&E staining of BAT in mice fed HFD at thermoneutrality (n = 6).
(G) Western blot analysis of UCP1 and OXPHOS complexes (CII-V) in BAT of mice fed HFD for 4 weeks at thermoneutrality (n = 6).
(H) Schematic model describing the role of ChREBP-dependent lipogenesis during BAT whitening.
Data are presented as means ± SEM. *$p < 0.05$ by ANOVA.
See also Figure S4.

KEY RESOURCES TABLE

REAGENT or RESOURCE	SOURCE	IDENTIFIER
Antibodies and Dilutions		
Rabbit polyclonal anti-AKT (1:1,000)	Cell Signaling	Cat# 9272; RRID: AB_329827
Rabbit polyclonal anti-ChREBP	Novus	Cat# NB400-135; RRID:AB_10002435
Mouse monoclonal anti-COX4 (1:5000)	Santa Cruz Biotechnology	Cat# sc-58348: RRID:AB_2229944
Rabbit polyclonal anti-LC3B (1:200)	Cell Signaling	Cat# 2775; RRID:AB_915950
Mouse OXPHOS WB cocktail (1:25,000)	Abcam	Cat# ab110413; RRID:AB_2629281
Rabbit polyclonal Phospho-PKA Substrate (RRXS/T) (1:1,000)	Cell Signaling	Cat# 9624; RRID:AB_331817
Rabbit monoclonal anti-gTubulin	Abcam	Cat# ab179503, RRID: N/A
Rabbit anti-UCP1 (1:12,500, IHC 1:1,000)	Cannon lab (Stockholm University)	N/A
HRP goat anti-mouse (1:5000)	Jackson ImmunoResearch Labs	Cat# 115-035-003; RRID:AB_10015289
HRP goat anti-rabbit (1:5000, IHC 1:500)	Jackson ImmunoResearch Labs	Cat# 111-035-144; RRID:AB_2307391
AF488-donkey-anti-rabbit (1:250)	Jackson Immunoresearch Labs	Cat# 711-546-152; RRID:AB_2340619
Chemicals and Reagents		
ACC inhibitor (CP-640186)	Sigma	Cat# PZ0362
ADP	Sigma	Cat# A2754
Antimycin A	Sigma	Cat# A8674
CCCP	Sigma	Cat# C2759
CL316,243	Tocris	Cat# 1499
cOmplete Mini Protease Inhibitor Cocktail	Roche	Cat# 1836153001
DAPI	Invitrogen	Cat# D1306
Eosin	Merck	Cat# 1.15935
EUKITT®	O. Kindler	N/A
GDP	Sigma	Cat# G7127
Hematoxylin	Sigma	Cat# MHS32-1L
Heparin	Rotexmedica	N/A
High-fat diet EF Bio-Serv	Sniff	Cat# F3282 mod
NuPAGE LDS 4x sample buffer	Invitrogen	Cat# NP0008
NuPAGE reducing sample buffer	Invitrogen	Cat# NP0004
Oligomycin	Sigma	Cat# O4876
Scintillation fluid	Zinsser Analytic	Cat# 1008500
Solvable™	Perkin Elmer	Cat# 6NE9100
SuperSignalWest Femto Substrate	Thermo Fisher	Cat# 34095
peqGOLD TriFast	peqlab	Cat# 30-2010
ProLong Gold antifade reagent	Invitrogen	Cat# P36930
Wortmannin	Calbiochem	Cat# 681675
^{3}H-Deoxyglucose	Hartmann Analytik	Cat# MT911
^{14}C-Triolein	Hartmann Analytik	Cat# ARC 0291

REAGENT or RESOURCE	SOURCE	IDENTIFIER
Critical Commercial Assays and Equipment		
Steady DAB/Plus	Abcam	Cat# ab103723
NucleoSpin RNA/Protein kit	Macherey & Nagel	Cat# 740933
High Capacity cDNA RT kit	Invitrogen	Cat# 4368813
TaqMan assay for *Acaca*	Thermo Fisher	Mm01304285_m1
TaqMan assay for *Acly*	Thermo Fisher	Mm00652520_m1
TaqMan assay for *Atp6*	Thermo Fisher	Mm03649417_g1
TaqMan assay for *Chrebpa*	Thermo Fisher	Mm01196407_m1
TaqMan assay for *Chrebpb*	Thermo Fisher	AIVI4CH
TaqMan assay for *Cox2*	Thermo Fisher	Mm03294838_g1
TaqMan assay for *Cox4i1*	Thermo Fisher	Mm00438289_g1
TaqMan assay for *Cox7a1*	Thermo Fisher	Mm00438297_g1
TaqMan assay for *Cox8b*	Thermo Fisher	Mm00432648_m1
TaqMan assay for *Cpt1b*	Thermo Fisher	Mm00487191_g1
TaqMan assay for *Dio2*	Thermo Fisher	Mm00515664_m1
TaqMan assay for *Elovl6*	Thermo Fisher	Mm00851223_s1
TaqMan assay for *Fasn*	Thermo Fisher	Mm00662319_m1
TaqMan assay for *Nd2*	Thermo Fisher	Mm04225288_s1
TaqMan assay for *Ppargc1a*	Thermo Fisher	Mm00447183_m1
TaqMan assay for *Scd1*	Thermo Fisher	Mm00772290_m1
TaqMan assay for *Srebf1*	Thermo Fisher	Mm00550338_m1
TaqMan assay for *Srebf2*	Thermo Fisher	Mm01306292_m1
TaqMan assay for *Srebp1c*	Thermo Fisher	AI89KJW
TaqMan assay for *Tbp*	Thermo Fisher	Mm00446973_m1
TaqMan assay for *Tfam*	Thermo Fisher	Mm00447485_m1
TaqMan assay for *Ucp1*	Thermo Fisher	Mm00494069_m1
Experimental Models: Organisms/Strains		
Mouse: C57BL/6J	The Jackson Laboratory	Stock No: 000664
Mouse: B6.129S6-Mlxipl^{tm1Kuy}/J	The Jackson Laboratory	Stock No: 010537
Mouse: B6.FVB-Tg(Ucp1-cre)1Evdr/J	The Jackson Laboratory	Stock No: 24670
Mouse: B6.129S4(FVB)-Insrtm1Khn/J	The Jackson Laboratory	Stock No: 006955
Mouse: B6.Tg(Ucp1-cre/ERT2)426Biat	Wolfrum lab (ETH)	Heine et al., 2018
Mouse: *Mlxipl$^{floxed/floxed}$*	Sleeman lab (Monash University)	Jois et al., 2017
Biological Samples		
Human BAT biopsies	Centre for Physical Activity Research, Rigshospitalet, University of Copenhagen, Denmark	Jespersen et al., 2020
Software		
Excel 2018 (Version 16.16.20)	Microsoft	RRID:SCR_016137
GraphPad Prism (Version 8.4.1)	GraphPad	RRID:SCR_002798

REAGENT or RESOURCE	SOURCE	IDENTIFIER
Image Studio Lite (Version 5.2.5)	LICOR	RRID:SCR_013715
NIS-Elements Advanced Research	NIKON	RRID:SCR_014329